2023

Fugacity-Based Lattice Boltzmann Method for Multicomponent Multiphase Systems

Muzammil Soomro

Luis F. Ayala

Cheng Peng

Orlando M. Ayala
Old Dominion University, oayala@odu.edu

Original Publication Citation

Soomro, M., Ayala, L. F., Peng, C., & Ayala, O. M. (2023). Fugacity-based lattice Boltzmann method for multicomponent multiphase systems. *Physical Review E, 107*(1), 1-20, Article 015304. https://doi.org/10.1103/PhysRevE.107.015304

Fugacity-based lattice Boltzmann method for multicomponent multiphase systems

Muzammil Soomro [*] and Luis F. Ayala
Department of Energy and Mineral Engineering, The Pennsylvania State University, University Park, Pennsylvania 16802, USA

Cheng Peng
Key Laboratory of High Efficiency and Clean Mechanical Manufacture, Ministry of Education, School of Mechanical Engineering, Shandong University, Jinan 250061, China

Orlando M. Ayala
Department of Engineering Technology, Old Dominion University, Norfolk, Virginia 23529, USA

(Received 8 September 2022; accepted 13 December 2022; published 17 January 2023)

The free-energy model can extend the lattice Boltzmann method to multiphase systems. However, there is a lack of models capable of simulating multicomponent multiphase fluids with partial miscibility. In addition, existing models cannot be generalized to honor thermodynamic information provided by any multicomponent equation of state of choice. In this paper, we introduce a free-energy lattice Boltzmann model where the forcing term is determined by the fugacity of the species, the thermodynamic property that connects species partial pressure to chemical potential calculations. By doing so, we are able to carry out multicomponent multiphase simulations of partially miscible fluids and generalize the methodology for use with any multicomponent equation of state of interest. We test this fugacity-based lattice Boltzmann method for the cases of vapor-liquid equilibrium for two- and three-component mixtures in various temperature and pressure conditions. We demonstrate that the model is able to reliably reproduce phase densities and compositions as predicted by multicomponent thermodynamics and can reproduce different characteristic pressure-composition and temperature-composition envelopes with a high degree of accuracy. We also demonstrate that the model can offer accurate predictions under dynamic conditions.

DOI: 10.1103/PhysRevE.107.015304

I. INTRODUCTION

Multiphase flows of fluids with multiple chemical components occur in many important settings like hydrocarbon reservoirs, carbon dioxide sequestration in aquifers, and chemical reactors. To achieve reliable modeling of these systems, it is essential to develop tools that can accurately model multicomponent multiphase (MCMP) flow, which would involve fluid dynamics coupling with thermodynamics. Under a thermodynamic framework, MCMP systems can be divided into two categories: Immiscible and partially miscible. In immiscible phases, some components in the system are confined to a single phase, and there is no interfacial mass transfer. In partially miscible phases, however, components can be exchanged between phases. An example of immiscible and partially miscible phases is shown in Fig. 1. It is worth noting that the terms immiscible and partially miscible are not applicable to single-component systems as a single-component multiphase system would always have to allow for interfacial mass transfer. Although modeling immiscible phases is quite popular, immiscibility is only a useful idealization meant to simplify modeling. There is always some degree of interfacial mass transfer in all multiphase systems; therefore, an accurate model for multiphase systems needs to account for partial miscibility.

In the study of partially miscible phases an equation of state (EOS) can play an important role. This is because in addition to relating the pressure of a system to its density, temperature, and composition, an EOS also contains information about the equilibrium state of multiphase systems. Therefore, the choice of EOS is crucial to the modeling of partially miscible fluids. Cubic EOSs, such as the Peng-Robinson (PR) [1] and the Soave-Redlich-Kwong (SRK) [2], are widely regarded as the most accurate ones to describe the thermodynamics of fluids. When multiple components are present, an EOS needs to account for interactions between "like" and "unlike" component pairs captured through mixing rules [3]. A realistic model of partially miscible systems, and hence MCMP systems, must incorporate an accurate EOS and the multicomponent mixing rules. The chemical potential governs the transport of a component within and across phases in MCMP systems. At equilibrium, the chemical potential of each component is constant throughout the multiphase system. In order to simplify phase equilibrium calculations, and to connect chemical potential and partial pressure calculations, the concept of fugacity was introduced [4]. At phase equilibrium, the equality of the fugacity of each component is mathematically equivalent to the equality of the chemical potential of each component. Although fugacity has primarily been used

[*] msoomro@psu.edu

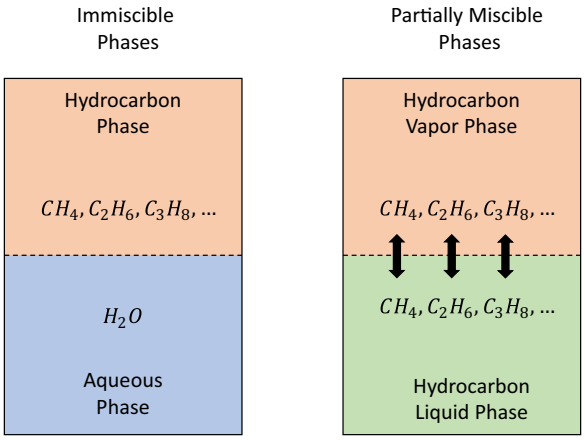

FIG. 1. Left: An immiscible system of a hydrocarbon phase composed of the components CH_4, C_2H_6, C_3H_8 among others and an aqueous phase composed of the component H_2O. The components are restricted to their phases and there is no interfacial mass transfer. Right: A partially miscible system of hydrocarbons with a light vapor phase and dense liquid phase. Both phases are composed of the same components (CH_4, C_2H_6, C_3H_8 among others) and there is interfacial mass transfer.

to simplify the phase equilibrium problem, it can also be a powerful quantity for simulating multiphase flow because it can be tied directly to an EOS. Thus, fugacity can be used as a bridge to incorporate accurate multicomponent EOSs into flow simulations.

Since the early 1990s, the lattice Boltzmann method (LBM) has emerged as a powerful fluid dynamics simulation tool with extensions to simulate multiphase flow. While early multiphase versions of LBM were restricted to studying the flow of immiscible fluids (e.g., Ref. [5]), models eventually emerged that allowed interfacial mass transfer, albeit only for single-component systems. Two of these models that have gained popularity are the pseudopotential model [6] and the free-energy model [7]. The pseudopotential model achieves phase separation by introducing a force to replicate intermolecular interactions, and it has been extended to incorporate any EOS [8]. It has also been extended to multicomponent systems of immiscible phases [9], and attempts have been made to consider multicomponent systems of partially miscible phases [10]. However, a well-known drawback of this method is its inconsistency with thermodynamics when using an EOS, which comes in two forms. The first inconsistency has to do with multicomponent versions of the pseudopotential LBM where a single-component EOS is used to calculate a pressure for each component [10]. The pressure is a property of a phase, not a component, and any multicomponent formulation should have one thermodynamic pressure at each point which comes from a multicomponent EOS with mixing rules. The second inconsistency applies to all pseudopotential models, and it is that at equilibrium, the fugacity of each component (as predicted by the EOS) is not constant throughout the system at equilibrium conditions [11]. In a single-component system, this is equivalent to violating the Maxwell equal area rule. While the first form of inconsistency can be addressed [12], the second form has only been fully resolved for single-component systems [13,14].

The free-energy model introduces macroscopic thermodynamics directly into lattice Boltzmann through a functional of the Helmholtz free energy [15], which makes it a good candidate for achieving full consistency with thermodynamics. While the free-energy model can be shown to be theoretically consistent with thermodynamics, it still does not lead to fully consistent simulations that can achieve full equality of chemical potentials and fugacities for phases in equilibrium [16]. Guo [17] showed that this inconsistency resulted from errors produced due to discretization, and the "well-balanced" LBM could eliminate these errors, making the free-energy model consistent with thermodynamics. Multiphase free-energy LBM has been used extensively with free-energy functionals that can be generalized to any EOS like the PR or SRK EOS but only for single-component (pure) systems [18–23]. Its extension to MCMP systems has mostly relied on the use of simpler free-energy functionals which can only qualitatively predict phase separation and are largely limited to immiscible MCMP systems [24–30]. In general, there remains a significant lack of models capable of performing LB simulations that fully honor multicomponent thermodynamics as predicted by multicomponent EOSs—including cases of systems of partial miscibility.

In this paper, we introduce a new free-energy LBM model which relies on the fugacity of each component, a property readily available through any EOS, to honor multicomponent thermodynamics fully. Through this new model, we can simulate flows of MCMP fluids with partial miscibility, using any multicomponent EOS. Additionally, by extending Guo's well-balanced LBM to multicomponent systems, we can show that our model fully complies with macroscopic thermodynamics and predicts phase densities and compositions in agreement with flash calculations done with the multicomponent EOS at a variety of different pressure and temperature conditions. Our paper is structured as follows. Section II will review the free-energy LBM and the limitations of previous models. In Sec. III, the fugacity-based LBM will be introduced, and the procedure to implement it will be shown. In Sec. IV, the fugacity-based LBM will be tested in various cases of vapor-liquid equilibrium, including tests for two-component and three-component mixtures and the generation of pressure-composition and temperature-composition envelopes. Additionally, the cases of spinodal decomposition and oscillating droplet will also be shown in this section. Finally, the main conclusions of the paper and discussions will be presented in Sec. V.

II. A REVIEW OF CURRENT FREE ENERGY LBM MODELS

LBM relies on the lattice Boltzmann equation (LBE) and for the case of a single-component fluid, this is given by Eq. (1) [31],

$$g_\alpha(\mathbf{r}+\mathbf{e}_\alpha\delta t, t+\delta t) - g_\alpha(\mathbf{r},t) = -\frac{1}{\tau}\left[g_\alpha(\mathbf{r},t) - g_\alpha^{(\mathrm{eq})}(\mathbf{r},t)\right] + \left[1-\frac{1}{2\tau}\right]F_\alpha(\mathbf{r},t)\delta t, \tag{1a}$$

$$g_\alpha^{(\mathrm{eq})} = \rho w_\alpha \left[1 + \frac{\mathbf{u}\cdot\mathbf{e}_\alpha}{c_s^2} + \frac{(\mathbf{u}\cdot\mathbf{e}_\alpha)^2}{2c_s^4} - \frac{\mathbf{u}\cdot\mathbf{u}}{2c_s^2} \right], \tag{1b}$$

$$F_\alpha = \mathbf{F}\cdot w_\alpha \left[\frac{\mathbf{e}_\alpha - \mathbf{u}}{c_s^2} + \frac{(\mathbf{u}\cdot\mathbf{e}_\alpha)\mathbf{e}_\alpha}{c_s^4} \right]. \tag{1c}$$

Here $\mathbf{r}$ is the position vector, $\mathbf{u}$ is the macroscopic velocity, $\mathbf{F}$ is the body force, c_s is the speed of sound, t is the time, τ is the relaxation time, ρ is the macroscopic mass density, and $\mathbf{e}_\alpha$, w_α, g_α, and $g_\alpha^{(\mathrm{eq})}$ are the lattice velocity, weighing parameter, distribution function and equilibrium distribution function for direction α, respectively. F_α is the forcing term given in Ref. [32]. It can be shown that at the macroscopic scale, LBE can replicate the Navier-Stokes equation [Eq. (2)] [32],

$$\frac{\partial}{\partial t}(\rho\mathbf{u}) + \nabla\cdot(\rho\mathbf{u}\mathbf{u}) = -\nabla\left(c_s^2\rho\right) + \nu\nabla\cdot\{\rho[\nabla\mathbf{u} + (\nabla\mathbf{u})^T]\} + \mathbf{F}. \tag{2}$$

Here ν is the kinematic viscosity, and the pressure is given by $c_s^2\rho$. The free energy model introduces multiphase thermodynamics into LBM by replacing the gradient of the standard LBM pressure, $c_s^2\rho$, with the divergence of an updated pressure tensor, $\overline{\overline{P}}$, in the Navier-Stokes equation. This pressure tensor contains the contributions from the bulk fluid, denoted by subscript B, and the interface, denoted by subscript I. To derive the pressure tensor, we need a functional of the Helmholtz free energy, referred to as the free-energy functional, and it is shown in Eq. (3),

$$\Psi(T,V,n) = \int \psi(T,\tilde{\rho})dV = \int (\psi_B + \psi_I)dV. \tag{3}$$

Here Ψ is the extensive free energy, which is a function of temperature (T), volume (V), and amount in moles (n) and ψ is the intensive free energy per unit volume which is a function of temperature and molar density ($\tilde{\rho}$). The chemical potential, μ, is then defined as the functional derivative of the extensive free energy with respect to moles (at constant T and V) or intensive free energy with respect to molar density (at constant T), as shown in Eq. (4),

$$\mu = \frac{\delta\Psi}{\delta n} = \frac{\delta\psi}{\delta\tilde{\rho}}. \tag{4}$$

Next, the divergence of the pressure tensor is calculated as a function of the gradient of the chemical potential through the application of the Gibbs-Duhem equation [Eq. (5)] for isothermal conditions,

$$\nabla\cdot\overline{\overline{P}} = \tilde{\rho}\nabla\mu. \tag{5}$$

The divergence of the pressure tensor is introduced into the LBE as a body force and this can either be done by the force in the "pressure form" [Eq. (6)] or the "potential form" [Eq. (7)] [33]. This body force will be input through Eq. (1c) and will appear in the Navier-Stokes equation [Eq. (2)],

$$\mathbf{F} = -\nabla\cdot\overline{\overline{P}} + \nabla\left(c_s^2\rho\right), \tag{6}$$

$$\mathbf{F} = -\tilde{\rho}\nabla\mu + \nabla\left(c_s^2\rho\right). \tag{7}$$

The term $\nabla(c_s^2\rho)$ in both forms of the force is an artificial term needed to cancel out the standard pressure gradient produced from the LBE at the Navier-Stokes level, leaving it only in terms of the real thermodynamic pressure. The interface free energy represents an energy penalty for having an interface and is expressed as $\psi_I = \frac{\kappa}{2}(\nabla\tilde{\rho})^2$ [34]. Through this expression, the "pressure form" and "potential form" of the force can be written as Eq. (8) and Eq. (9), respectively [17,33],

$$\mathbf{F} = -\nabla p_B + \kappa\tilde{\rho}\nabla(\nabla^2\tilde{\rho}) + \nabla\left(c_s^2\rho\right), \tag{8}$$

$$\mathbf{F} = -\tilde{\rho}\nabla\mu_B + \tilde{\rho}\nabla(\kappa\nabla^2\tilde{\rho}) + \nabla\left(c_s^2\rho\right). \tag{9}$$

Here κ is a parameter controlling interfacial tension strength, and p_B and μ_B are the bulk (without contributions from the interface) pressure and chemical potential, respectively. Theoretically, the free-energy model is supposed to be consistent with thermodynamics (it should fulfill the isofugacity criterion at equilibrium); however, Guo [17] showed that due to the different discretizations involved in the LBE and the body force, the $\nabla(c_s^2\rho)$ term does not entirely cancel out. To solve this, the "well-balanced" LBM was introduced with the equilibrium distribution function and forcing term given by Eq. (10) and Eq. (11), respectively,

$$g_\alpha^{(\mathrm{eq})} = \begin{cases} \rho - (1-w_0)\rho_0 + w_0\rho\left[\frac{\mathbf{u}\cdot\mathbf{e}_\alpha}{c_s^2} + \frac{(\mathbf{u}\cdot\mathbf{e}_\alpha)^2}{2c_s^4} - \frac{\mathbf{u}\cdot\mathbf{u}}{2c_s^2}\right] & \text{if } \alpha = 0 \\ w_\alpha\rho_0 + w_\alpha\rho\left[\frac{\mathbf{u}\cdot\mathbf{e}_\alpha}{c_s^2} + \frac{(\mathbf{u}\cdot\mathbf{e}_\alpha)^2}{2c_s^4} - \frac{\mathbf{u}\cdot\mathbf{u}}{2c_s^2}\right] & \text{if } \alpha \neq 0 \end{cases}, \tag{10}$$

$$F_\alpha = \mathbf{F}\cdot w_\alpha\left[\frac{\mathbf{e}_\alpha - \mathbf{u}}{c_s^2} + \frac{(\mathbf{u}\cdot\mathbf{e}_\alpha)\mathbf{e}_\alpha}{c_s^4}\right] + \nabla\rho\cdot w_\alpha\left[-\mathbf{u} + \frac{(\mathbf{u}\cdot\mathbf{e}_\alpha)\mathbf{e}_\alpha}{c_s^2} + \frac{1}{2}\left(\frac{\mathbf{e}_\alpha^2}{c_s^2} - D\right)\mathbf{u}\right]. \tag{11}$$

Here ρ_0 is a numerical constant set to 0 as suggested by Guo [17] and D is the spacial dimension of the problem. With this new formulation, the artificial $\nabla(c_s^2\rho)$ term does not need to be included in Eqs. (8) and (9).

Single-component free-energy models allow for interfacial mass transfer and have been able to successfully incorporate EOSs through both the pressure form [18–20] and potential form [21–23] of the force. For the pressure form, this is straightforward as the pressure p_B, in Eq. (8), is simply provided through the EOS. For the potential form, the intensive free energy per unit volume, $\psi(T,\tilde{\rho})$, is first obtained for an isothermal case through an EOS by solving the ordinary

differential equation given by Eq. (12) to obtain the general solution given by Eq. (13) [21],

$$\psi_B - \tilde{\rho}\frac{d\tilde{\psi}_B}{d\tilde{\rho}} - p_B = 0, \tag{12}$$

$$\psi_B = \tilde{\rho}\left[\int \frac{p_B}{\tilde{\rho}^2} d\tilde{\rho} + C\right]. \tag{13}$$

Here C is a temperature-dependent constant of integration. Then the chemical potential is found, again for an isothermal case, as the derivative of the intensive free energy with respect to the molar density [21].

However, neither the approach for incorporating an EOS through the pressure form nor the potential form can be extended to multicomponent fluids. For a multicomponent fluid, the LBM requires a forcing term for each component, as shown later in Sec. III, and therefore a body force must be derived for each component. Equation (8), used to calculate the force in the pressure form, cannot be written for each component as dividing the pressure gradient between components would not be physically meaningful since pressure is a property of the phase and not the component. Equation (9) for the potential form, on the other hand, can be written for each component as the chemical potential is a property of the component and is the natural variable that drives mass transfer for each component. However, for a multicomponent case, the intensive free energy cannot be derived the same way as for a single-component case. This is because the intensive free energy for a multicomponent system is a function of temperature and molar density of each component, $\tilde{\rho}_i$ ($\tilde{\rho}_i = n_i/V$, where n_i is the moles of component i). Integrating an EOS will produce a constant of integration that depends not only on the temperature but also on the fluid composition, which is not constant throughout the system. Detailed analysis and discussion of this argument are given in Appendix A.

Multicomponent extensions of the free-energy model do exist and have primarily been restricted to two-component systems [24,25], with some extensions being to three-component systems [26,27] and some being applicable to any number of components [28–30]. While majority of these models are for immiscible phases, there have been extensions to partially miscible phases in the context of phase field modeling [35,36]. However, these models rely on simple free-energy models with the "multiwell" geometry needed to trigger phase separation. They may qualitatively predict phase separation but they will not offer quantitatively accurate predictions of phase density and composition. Recently, Ridl and Wagner [37] introduced a multicomponent model for partially miscible systems based on the multicomponent van der Waals (vdW) EOS. vdW fluids have a theoretical basis in statistical mechanics, through which their free-energy functional can be derived [38]. However, this approach does not apply to any EOS in general due to their empirical nature, as demonstrated in Appendix B. Wöhrwag *et al.* [39] introduced a ternary fluid model applicable to any single-component EOS. They introduced a free-energy model using a combination of single-component EOS and qualitative "double-well" potentials. However, single-component EOSs do not apply to multicomponent mixtures. For a multicomponent mixture, interactions between like and unlike component pairs are captured through mixing rules, and these are not accounted for in a single-component EOS. Common EOSs and multicomponent mixing rules are given in Appendix C. There is a lack of LBM models equipped to deal with partially miscible MCMP fluids, which can additionally incorporate any multicomponent EOS, and that is what we aim to address with the proposed fugacity-based LBM. Some important studies discussed in this section and their limitations have been summarized in Table I, along with the aim of the proposed fugacity-based LBM model, which will be introduced in Sec. III.

III. THE FUGACITY-BASED LATTICE BOLTZMANN METHOD

A. Theory

To solve problems involving MCMP mixtures with a greater degree of accuracy, we introduce a new approach to the free-energy model, with a body force for each component i ($\mathbf{F}_i$) based on the fugacity of component i (f_i). For the well-balanced LBM formulation, this force is shown in Eq. (14),

$$\mathbf{F}_i = -\tilde{\rho}_i RT \nabla \ln f_i - \tilde{\rho}_i \nabla \mu_{I,i}. \tag{14}$$

Here R is the universal gas constant and $\mu_{I,i}$ is the interface chemical potential for component i. Since this force is to be used with the well-balanced LBM, there will be no artificial term to cancel out the standard pressure from the LBE. However, if the standard LBM formulation is used, then Eq. (14) should have an additional $c_s^2 \nabla \rho_i$ term added to it. In order to arrive at Eq. (14), we start by extending the well-balanced LBM formulation for a multicomponent system; the well-balanced LBE for a component i is given by Eq. (15),

$$g_{\alpha,i}(\mathbf{r}+\mathbf{e}_\alpha\delta t, t+\delta t) - g_{\alpha,i}(\mathbf{r},t) = -\frac{1}{\tau}\left[g_{\alpha,i}(\mathbf{r},t) - g^{(\mathrm{eq})}_{\alpha,i}(\mathbf{r},t)\right] + \left[1-\frac{1}{2\tau}\right]F_{\alpha,i}(\mathbf{r},t)\delta t, \tag{15a}$$

$$g^{(\mathrm{eq})}_{\alpha,i} = \begin{cases} \rho_i - (1-w_0)\rho_0 + w_0\rho_i\left[\frac{\mathbf{u}\cdot\mathbf{e}_\alpha}{c_s^2} + \frac{(\mathbf{u}\cdot\mathbf{e}_\alpha)^2}{2c_s^4} - \frac{\mathbf{u}\cdot\mathbf{u}}{2c_s^2}\right] & \text{if } \alpha = 0 \\ w_\alpha\rho_{0,i} + w_\alpha\rho_i\left[\frac{\mathbf{u}\cdot\mathbf{e}_\alpha}{c_s^2} + \frac{(\mathbf{u}\cdot\mathbf{e}_\alpha)^2}{2c_s^4} - \frac{\mathbf{u}\cdot\mathbf{u}}{2c_s^2}\right] & \text{if } \alpha \neq 0 \end{cases}, \tag{15b}$$

$$F_{\alpha,i} = \mathbf{F}_i \cdot w_\alpha\left[\frac{\mathbf{e}_\alpha - \mathbf{u}}{c_s^2} + \frac{(\mathbf{u}\cdot\mathbf{e}_\alpha)\mathbf{e}_\alpha}{c_s^4}\right] + \nabla\rho_i \cdot w_\alpha\left[-\mathbf{u} + \frac{(\mathbf{u}\cdot\mathbf{e}_\alpha)\mathbf{e}_\alpha}{c_s^2} + \frac{1}{2}\left(\frac{\mathbf{e}_\alpha^2}{c_s^2} - D\right)\mathbf{u}\right]. \tag{15c}$$

TABLE I. Selected studies from Sec. II categorized by relevant features and the aim of the proposed fugacity-based LBM.

Model	Can handle multiple components	Can incorporate any equation of state	Allows partial miscibility (for multicomponent models)	Applies mixing rules (for multicomponent models)
Mazloomi M. *et al.* [19]	✗	✓	–	–
Siebert *et al.* [20]	✗	✓	–	–
Wen *et al.* [21]	✗	✓	–	–
Liang *et al.* [26]	✓	✗	✗	✗
Yuan *et al.* [28]	✓	✗	✗	✗
Zheng *et al.* [29]	✓	✗	✗	✗
Ridl and Wagner [37]	✓	✗	✓	✓
Wöhrwag *et al.* [39]	✓	✓	✗	✗
Proposed model	✓	✓	✓	✓

Here $\rho_{0,i}$ will be set to 0 as in the single-component formulation. The forcing term for each component, given by Eq. (15c), requires a body force for each component. For this, we write the potential form of the body force for each component [37,40] as shown in Eq. (16). Again, the force will not have the artificial $c_s^2\nabla\rho_i$ term because of the use of the well-balanced LBM,

$$\mathbf{F}_i = -\tilde{\rho}_i \nabla \mu_i. \tag{16}$$

The chemical potential for component i is defined as the functional derivative of the extensive free energy with respect to moles of i (at constant T, V, and $n_{j\neq i}$) or intensive free energy with respect to molar density of i (at constant T and $\tilde{\rho}_{j\neq i}$), as shown in Eq. (17). Writing the free energy in terms of its contribution from the bulk fluid and the interface, as shown in Eq. (3), the chemical potential for component i can also be split into its bulk and interface contributions as in Eq. (18),

$$\mu_i = \frac{\delta\Psi}{\delta n_i} = \frac{\delta\psi}{\delta\tilde{\rho}_i}, \tag{17}$$

$$\mu_i = \mu_{B,i} + \mu_{I,i}, \tag{18a}$$

$$\mu_{B,i} = \frac{\partial\psi_B}{\partial\tilde{\rho}_i}, \tag{18b}$$

$$\mu_{I,i} = \frac{\delta\psi_I}{\delta\tilde{\rho}_i}. \tag{18c}$$

As seen in Eq. (18b), the bulk chemical potential would require a multicomponent free-energy functional, which is not available for all EOSs (e.g., the PR and SRK EOS). However, this free-energy functional is no longer needed if we use a formulation based on the fugacity, a property readily available for any EOS. The fugacity of component i is defined using the differential given by Eq. (19a) and the reference state given by Eq. (19b) [4],

$$d\ln f_i \equiv \frac{d\mu_{B,i}}{RT} \quad \text{at const } T, \tag{19a}$$

$$\lim_{p\to 0}\frac{f_i}{x_i p} \equiv 1. \tag{19b}$$

Using Eq. (19a), the gradient of the bulk chemical potential for an isothermal system can be written as:

$$\nabla\mu_{B,i} = RT\nabla\ln f_i. \tag{20}$$

Splitting Eq. (16) into its bulk and interface contributions and using Eq. (20), we can arrive at our proposed form of the force, Eq. (14). An expression for the fugacity of component i can be obtained by integrating Eq. (19a) and using the reference state given by Eq. (19b) and then this expression can be evaluated using an EOS as shown in Appendix C.

To perform MCMP simulations, we still require the interface chemical potential. The interface chemical potential should represent an energy penalty for having an interface. Several multicomponent models exist for the interface free energy from which the interface chemical potential can be derived [30,39,41]. However, this paper will use the interface free energy given by Ridl and Wagner [37] since it considers the interactions between component pairs, which is crucial for partially miscible phases. According to this interface free energy, the interface chemical potential is given by Eq. (21),

$$\mu_{I,i} = -\sum_{j=1}^{N_c}(\kappa_{ij}\nabla^2\tilde{\rho}_j), \tag{21}$$

where κ_{ij} controls the strength of the interfacial tension and comes from the molecular interactions between component i and component j. Since κ_{ij} comes from intermolecular interactions, we can calculate its value through van der Waals mixing rules [similarly to Eq. (C2b) in Appendix C] using pure component strength of interfacial tension, κ_i, as shown in Eq. (22),

$$\kappa_{ij} = \sqrt{\kappa_i\kappa_j}. \tag{22}$$

The pure component interfacial tension strengths can be adjusted to achieve the desired interfacial tension in the system. In general, the less volatile a component, the greater the intermolecular forces and hence the greater the surface tension. Therefore, for a pure component, the lower the volatility, the greater the value of κ_i. With this, the final form of the force can be written as shown in Eq. (23),

$$\mathbf{F}_i = -\tilde{\rho}_i RT\nabla\ln f_i + \tilde{\rho}_i\sum_{j=1}^{N_c}\nabla(\sqrt{\kappa_i\kappa_j}\,\nabla^2\tilde{\rho}_j). \tag{23}$$

B. Implementation

The proposed model will require the calculation of the gradient and Laplacian for certain properties, which will require

approximating the first- and second-order spatial derivatives of those properties. For this study, the following finite-difference schemes will be used to evaluate the derivatives for any generic property h and the direction x:

$$\frac{dh}{dx} \approx \frac{h(x+\delta x) - h(x-\delta x)}{2\delta x}, \tag{24}$$

$$\frac{d^2h}{dx^2} \approx \frac{h(x+\delta x) - 2h(x) + h(x-\delta x)}{\delta x^2}. \tag{25}$$

The procedure to implement the fugacity-based LBM is straightforward and outlined as follows.

(1) Given the distribution functions and body forces of each component at a particular lattice node from the previous time step, compute the component mass density ρ_i, total mass density ρ, and velocity $\mathbf{u}$ at that lattice node, using the following equations:

$$\rho_i = \sum_\alpha g_{\alpha,i}; \quad \rho = \sum_i \rho_i; \quad \mathbf{u} = \frac{1}{\rho}\sum_i \left[\sum_\alpha g_{\alpha,i}\mathbf{e}_\alpha + \frac{\mathbf{F}_i\delta t}{2}\right].$$

(2) Calculate the component molar density $\tilde{\rho}_i$, the total molar density $\tilde{\rho}$, and component mole fraction (or composition) x_i, using the following relations:

$$\tilde{\rho}_i = \frac{\rho_i}{M_i}; \quad \tilde{\rho} = \sum_i \tilde{\rho}_i; \quad x_i = \frac{\tilde{\rho}_i}{\tilde{\rho}},$$

where M_i is the molar mass of component i.

(3) Apply the mixing rules to obtain the attraction parameter for the mixture (a_m for vdW or $a\alpha_m$ for SRK and PR EOS) and covolume for the mixture (b_m). This process is outlined in Appendix C.

(4) Obtain the pressure through an EOS [the vdW, SRK, and PR EOS are given in Appendix C by Eqs. (C1), (C4), and (C6), respectively].

(5) Obtain the natural log of fugacity for each component, $\ln f_i$, using a fugacity expression relevant to the EOS used [the fugacity expressions for vdW, SRK, and PR EOS are given in Appendix C by Eqs. (C15), (C16), and (C17), respectively].

(6) Obtain the interface chemical potential using Eq. (21). Use Eq. (25) when evaluating the second-order spatial derivatives to calculate the Laplacian of the component molar density.

(7) Calculate the body force for each component as given by Eq. (14). Use Eq. (24) to evaluate the first-order space derivatives when calculating the gradient of relevant properties.

(8) Calculate the equilibrium distribution function and forcing term for each component using Eqs. (15b) and (15c), respectively.

(9) Perform collision for each component followed by propagation for each component to obtain the new distribution functions. Repeat steps 1–9 until the simulation is run for the desired time.

IV. RESULTS

To test the fugacity-based LBM, we perform several simulations on a two-phase vapor-liquid equilibrium system with the phases separated by a flat interface and compare the simulation results to those predicted by a flash calculation. We start by testing whether the model works for different EOSs by simulating a two-component mixture using the PR and SRK EOS. Next, the model is tested for a two-component mixture under various pressure and temperature conditions, and the pressure-composition and the temperature-composition envelopes are generated. Finally, a three-component mixture is simulated to show that the model can be extended to any number of components. After testing the cases of vapor liquid equilibrium, we simulate the case of a uniform system undergoing spinodal decomposition to form two separate phases and validate our results by testing the equality of component fugacity in each phase. Last, we test our model under dynamic conditions by simulating the case of an oscillating droplet, and comparing the obtained oscillation period with its theoretical value. Different mixtures were created for each case from the components listed in Table II.

For all the simulations, a D2Q9 lattice is used in a periodic computational domain, and the relevant conversions between lattice units and physical units are established by fixing the universal gas constant and the attraction parameter, covolume, and molar mass for the most volatile component in each mixture to the following values: $R = 1$, $a_i = 2/49$, $b_i = 2/21$, and $M_i = 1$. In Table II, the volatility decreases from methane to n-pentane. The binary interaction parameter between each component pair is 0.

A. Two-component mixture using PR and SRK equations of state

In this case, we will simulate a system of propane (C3) and n-pentane (C5) at equilibrium using the PR and SRK EOS, with the mole fraction of C3 and C5 in the system being 0.4 and 0.6, respectively. For reference, a flat interface, vapor-liquid equilibrium case using these two components has been carried out in Ref. [12] with the PR EOS [the results are shown in Figs. 5(c) and 5(d) of Ref. [12]]. However, in Ref. [12], two additional parameters were needed to achieve the isofugacity criterion: a force split coefficient (γ) depending on the pressure and temperature and a tuning parameter (β). We will show that the fugacity-based LBM can achieve similar results under similar conditions without needing any tuning or empirical parameters. The simulations are initialized at a pressure of 16.547 bar (240 psia) and a temperature of 370.03 K (666.06°R). The size of the computational domain is 400×2 ($n_x \times n_y$), the relaxation time $\tau = 0.8$ and the values interfacial tension strength are $\kappa_{C1} = 0.10$ and $\kappa_{C5} = 0.15$. The density of each component in the x direction is initialized as shown in Eq. (26) (the domain will be symmetric in the y direction),

$$\rho_i(x, t=0) = \rho_{i,V} + \frac{\rho_{i,L} - \rho_{i,V}}{2}\left(\tanh\left[\frac{2\left(x - \frac{S_V}{2}n_x\right)}{W}\right] - \tanh\left\{\frac{2\left[x - \left(1 - \frac{S_V}{2}\right)n_x\right]}{W}\right\}\right). \tag{26}$$

Here W is the initial interface width set to be 8 and $\rho_{i,V}$, $\rho_{i,L}$, and S_V are the density of component i in the vapor phase, density of component i in the liquid phase and saturation (volume fraction) of the vapor phase, respectively, which are calculated

TABLE II. The properties of relevant components used in the LBM simulations.

Component	Critical pressure (bar)	Critical temperature (K)	Accentric factor	Molar mass (g/mol)
Methane (C1)	45.947	190.74	0.0104	16.043
Ethane (C2)	48.711	305.51	0.0979	30.070
Propane (C3)	42.472	370.03	0.1522	44.097
n-pentane (C5)	33.688	469.89	0.2514	72.150

by performing a flash calculation for the given mixture at $p = 16.547$ bar and $T = 370.03$ K using the relevant EOS. The simulations are run for 1 000 000 time steps to achieve equilibrium, and the density and composition (mole fractions) versus the dimensionless length (x/n_x) are shown in Fig. 2 and Fig. 3 for the PR and SRK EOS, respectively. The results predicted from a flash calculation using the relevant EOS are also included in the figures. It should be noted that when initializing the densities using Eq. (26), the equilibrium values of densities at the given pressure and temperature conditions are used in the bulk vapor and liquid regions. However, the densities at the interface are only approximations of the equilibrium state, as the exact equilibrium profile at the interface is not given by the "tanh" profile. As a result, a new equilibrium

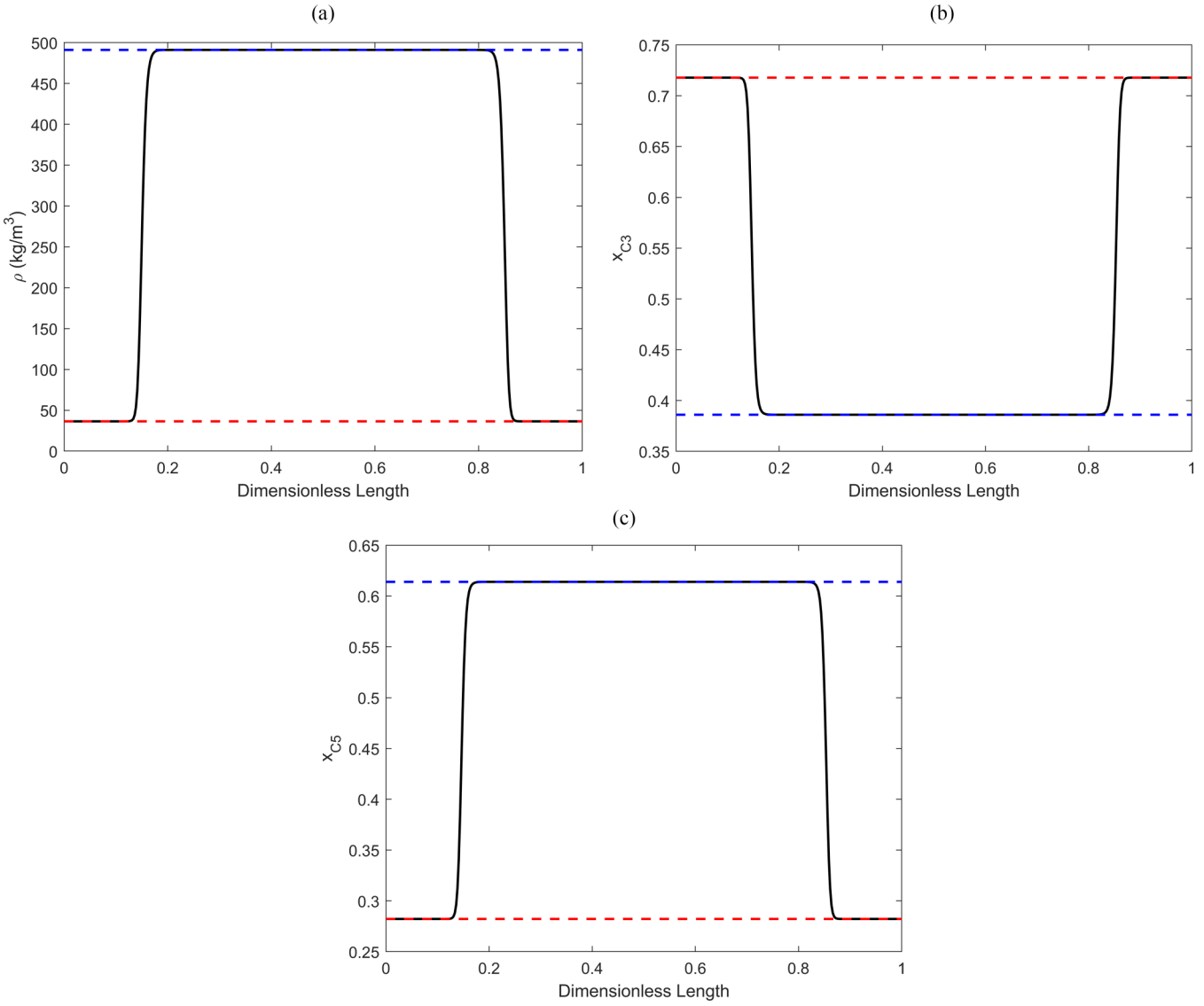

FIG. 2. The equilibrium profiles for (a) density, (b) composition of C3, and (c) composition of C5 using the PR EOS. The solid black line shows the results from LBM and the dashed blue and red lines show the theoretical values from a flash calculation for the liquid and vapor phase, respectively.

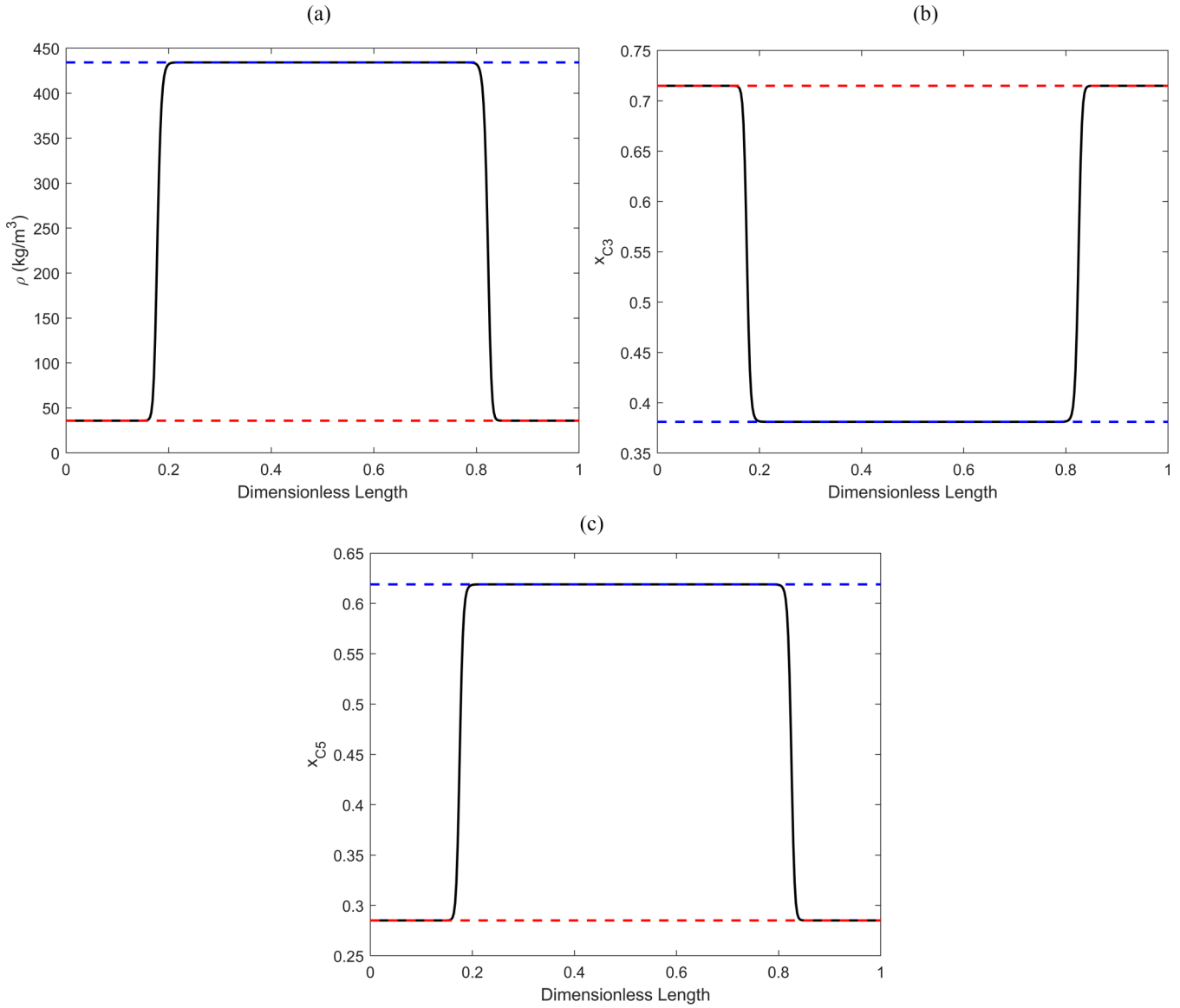

FIG. 3. The equilibrium profiles for (a) density, (b) composition of C3, and (c) composition of C5 using the SRK EOS. The solid black line shows the results from LBM and the dashed blue and red lines show the theoretical values from a flash calculation for the liquid and vapor phase, respectively.

will be reached where the pressure will slightly deviate from 13.79 bar. The LBM simulations are compared with flash calculations at the updated pressures.

The deviation of the fugacity-based LBM results from the flash calculation results is quantified with a relative error percentage:

$$\text{Relative Error } (\%) = \frac{|z^{\text{LBM}} - z^{\text{Theory}}|}{z^{\text{Theory}}} \times 100\%, \qquad (27)$$

where z is the property to be measured (density or composition). The errors are tabulated in Table III. As can be seen from the error values, a near exact match between the LBM results and theoretical results is obtained.

B. Pressure-composition and temperature-composition envelopes

For this case, we will investigate the phase behavior of a two-component system at different pressure and temperature conditions and create the pressure-composition (p-x) and temperature-composition (T-x) envelopes. We consider an ethane (C2) and pentane (C5) system and use the PR EOS. The pressure-temperature (p-T) envelopes of this system at different compositions (mole fractions) of C2 generated using the PR EOS are shown in Fig. 4(a). The critical locus, which is the curve connecting all the critical points of the mixtures at different compositions, along with the saturation curves for pure C2 and pure C5, bound the possible two-phase region on the p-T plane. For a p-x envelope, flash calculations are performed for different pressures at a constant temperature and

TABLE III. The relative error values in the density, C3 composition and C5 composition in the different phases and with different EOSs.

Property	Liquid region error using PR (%)	Vapor region error using PR (%)	Liquid region error using SRK (%)	Vapor region error using SRK (%)
Density	1.70×10^{-5}	1.40×10^{-4}	4.27×10^{-5}	3.00×10^{-4}
x_{C3}	7.94×10^{-7}	4.69×10^{-6}	2.62×10^{-6}	1.27×10^{-6}
x_{C5}	4.99×10^{-7}	1.19×10^{-5}	1.61×10^{-6}	3.17×10^{-6}

the composition of C2 in the vapor phase ($x_{C2,V}$) and liquid phase ($x_{C2,L}$) are recorded. A plot of pressure versus $x_{C2,V}$ will make the dew point curve, whereas a plot of pressure versus $x_{C2,L}$ will make the bubble point curve. For a T-x envelope, this process is repeated with the pressure held constant, and the vapor and liquid compositions plotted with temperature. Different characteristic plots can be produced depending on the choice of the isotherm for a p-x plot or the choice of isobar for the T-x plot. Several different isotherms and isobars of interest which will be tested are shown in Fig. 4(b).

In Fig. 4(b), we see two isotherms $T_1 = 274.96$ K and $T_2 = 387.70$ K such that $T_1 < T_{c,C2} < T_{c,C5}$ and $T_{c,C2} < T_2 < T_{c,C5}$. At T_1 the p-x envelope will begin from $x_{C2} = 0$ and end at $x_{C2} = 1$. However, at T_2, the p-x envelope will begin from $x_{C2} = 0$ and end before reaching $x_{C2} = 1$. We perform several simulations at different pressures and a fixed temperature to replicate this behavior with the fugacity-based LBM. A 200×2 ($n_x \times n_y$) computational domain is used, with the relaxation time $\tau = 1.25$ and the values interfacial tension strength being $\kappa_{C2} = 0.1$ and $\kappa_{C5} = 0.2$. The density is initialized using Eq. 26 with $W = 4$ and $\rho_{i,V}$ and $\rho_{i,L}$ calculated from a flash calculation at the respective initial pressure and temperature. The overall composition in the system is chosen such that $S_V = 0.5$ for all simulations. For a binary system, this will not impact the values of phase compositions. Each simulation is run for 500 000 time steps to ensure equilibrium is reached. The theoretical p-x envelope generated by performing flash calculations using the PR EOS and the p-x envelope generated by plotting the equilibrium values of pressure and phase composition from the fugacity-based LBM are shown in Figs. 5(a) and 5(c). In order to show the deviation of the values of compositions predicted by the fugacity-based LBM at a certain pressure from the theoretical values, the relative errors are calculated using Eq. (27). The relative error versus pressure plots are shown in Figs. 5(b) and 5(d). It can be seen that the error lies between the order of magnitude of 1% to 10^{-8}% indicating excellent agreement between the theoretical and predicted values. Again, this excellent agreement is achieved without any type of user intervention, tuning, or empirical manipulation.

Next, this process is repeated at constant pressure to create T-x envelopes. Figure 4(b) shows three relevant isobars $p_1 = 30$ bar, $p_2 = 45$ bar, and $p_3 = 58$ bar such that $p_1 < p_{c,C5} < p_{c,C2}$, $p_{c,C5} < p_2 < p_{c,C2}$, and $p_{c,C5} < p_{c,C2} < p_3$. At p_1 the T-x envelope will begin from $x_{C2} = 0$ and end at $x_{C2} = 1$, at p_2 the T-x envelope will begin after $x_{C2} = 0$ and end at $x_{C2} = 1$, and at p_3 the T-x envelope will begin after $x_{C2} = 0$ and end before $x_{C2} = 1$. This behavior is replicated using the fugacity-based LBM using the same values of n_x, n_y, τ, κ_{C2}, κ_{C5}, W, S_V and the number of time steps as those used to generate the p-x envelopes. The temperature is varied at a given pressure, and $\rho_{i,V}$ and $\rho_{i,L}$ are initialized accordingly. The theoretical T-x envelope generated by performing flash calculations using the PR

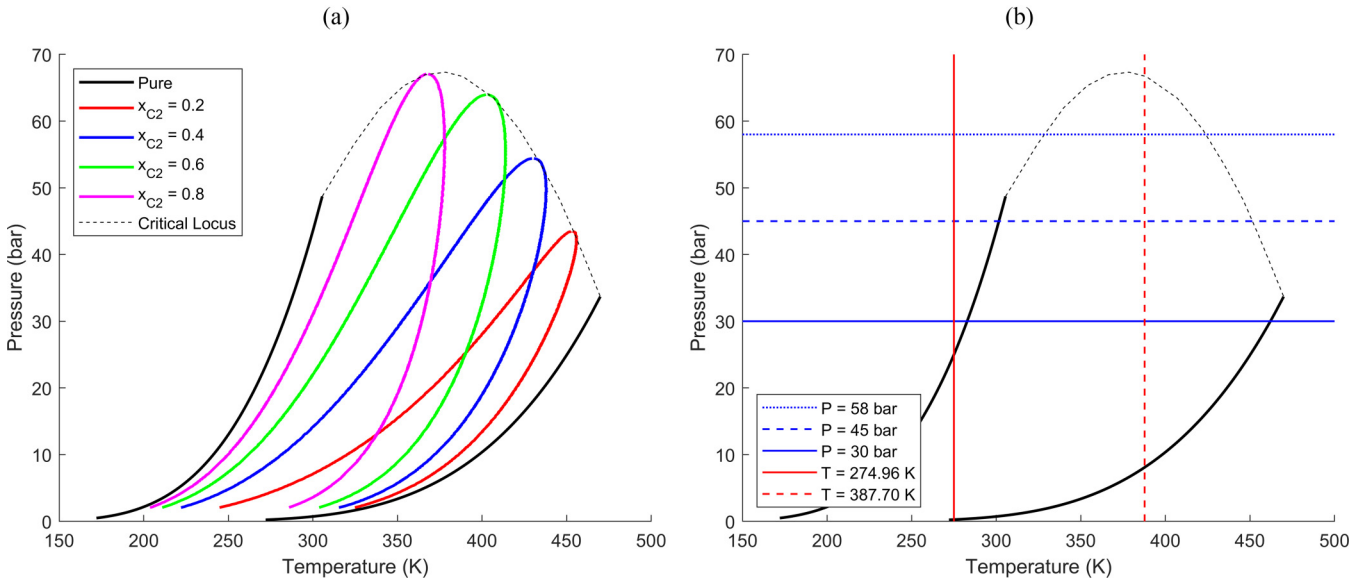

FIG. 4. (a) The pressure-temperature envelopes for the C2-C5 mixture at different compositions of C2. The solid black lines represent the pure species with the line on the right representing pure C5 and the line on the left representing pure C2. (b) The black lines are the pure component curves and critical locus from (a), the blue lines represent the relevant isobars and the red lines represent the relevant isotherms.

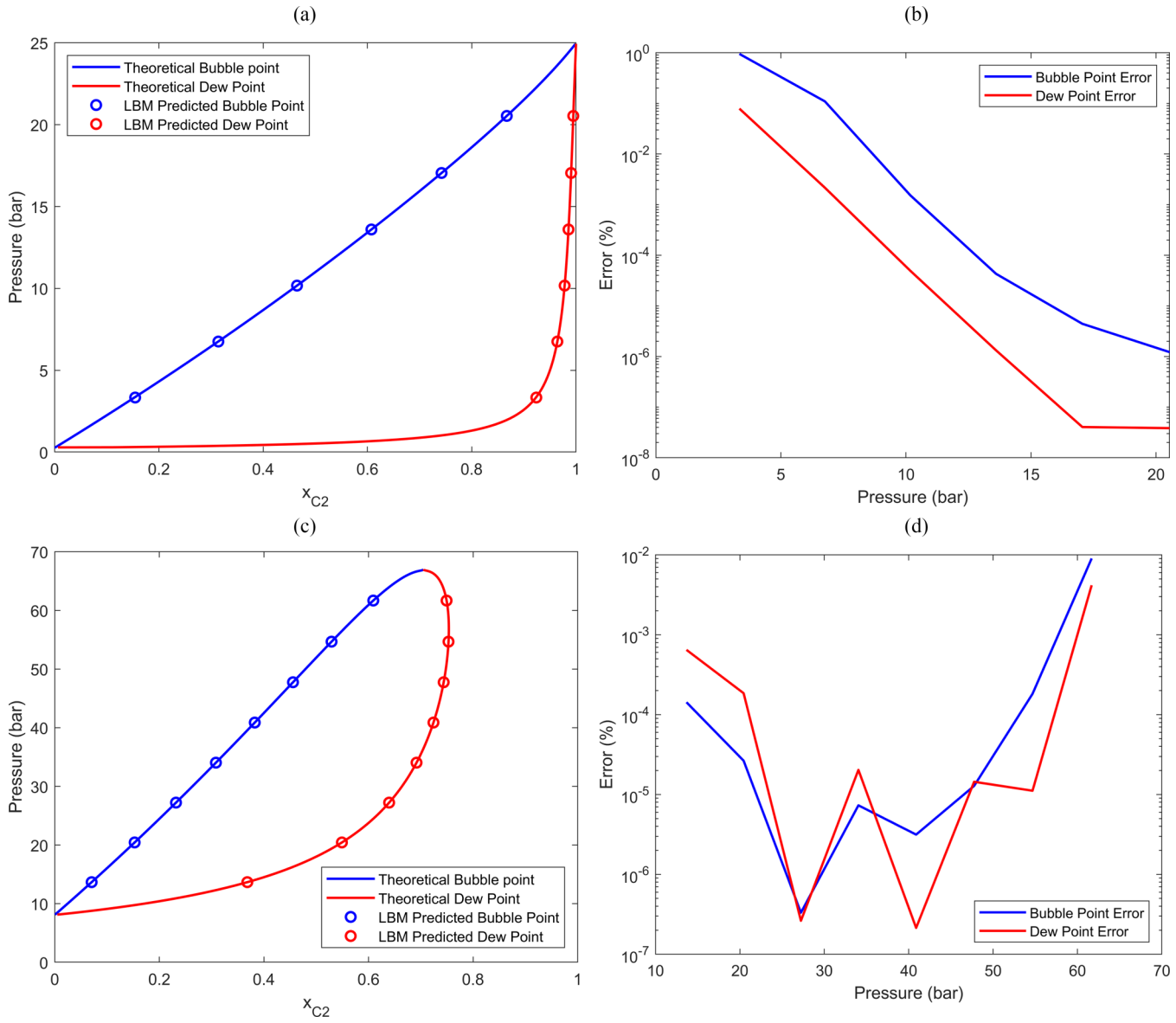

FIG. 5. Left: The p-x envelopes at (a) $T = 274.96$ K and (c) $T = 387.70$ K, where the solid lines represent the theoretical results and the dots represent the results predicted by LBM. Right: The relative error (%) in the predicted values at (b) $T = 274.96$ K and (d) $T = 387.70$ K.

EOS and the T-x envelope generated by plotting the equilibrium values of temperature and phase composition from the fugacity-based LBM are shown in Figs. 6(a), 6(c), and 6(e). The deviation of the predicted values from the theoretical ones is slightly greater for the T-x envelope than for the p-x envelope. This is because for the T-x envelope, we are assuming that the pressure remains constant at its initial value (at p_1, p_2, or p_3) for each temperature condition in the envelope. However, the pressure deviates slightly from the initial value as the initialization is not done at the true equilibrium because of the "tanh" interface approximation as discussed in Sec. IV A. When the errors at each temperature are calculated using the theoretical values of composition at the actual equilibrium pressure (and not the pressure of the chosen isobar), the error versus temperature graphs are shown in Figs. 6(b), 6(d), and 6(f). The errors range in orders of magnitude from 10^{-2}% to 10^{-8}%, again showing excellent agreement between predicted and theoretical results.

For the reader's reference, the equivalent vapor and liquid phase density versus pressure plots for the simulations in Fig. 5 and the equivalent vapor and liquid phase density versus temperature plots for the simulations in Fig. 6 are shown in Appendix D.

C. Three-component mixtures

In this section, we show that our formulation is not restricted to binary mixtures by simulating the two-phase vapor-liquid system with a flat interface using three components. Methane (C1), ethane (C2), and propane (C3) with the overall mole fractions 0.4, 0.3, and 0.3, respectively, are chosen for this case. The PR EOS is used. The size of the computational domain is 200×2 ($n_x \times n_y$), the relaxation time $\tau = 1$, and the values of interfacial tension strength are $\kappa_{C1} = 0.05$, $\kappa_{C2} = 0.10$, and $\kappa_{C3} = 0.15$. The system is initialized at a temperature of 216.483 K and a pressure of

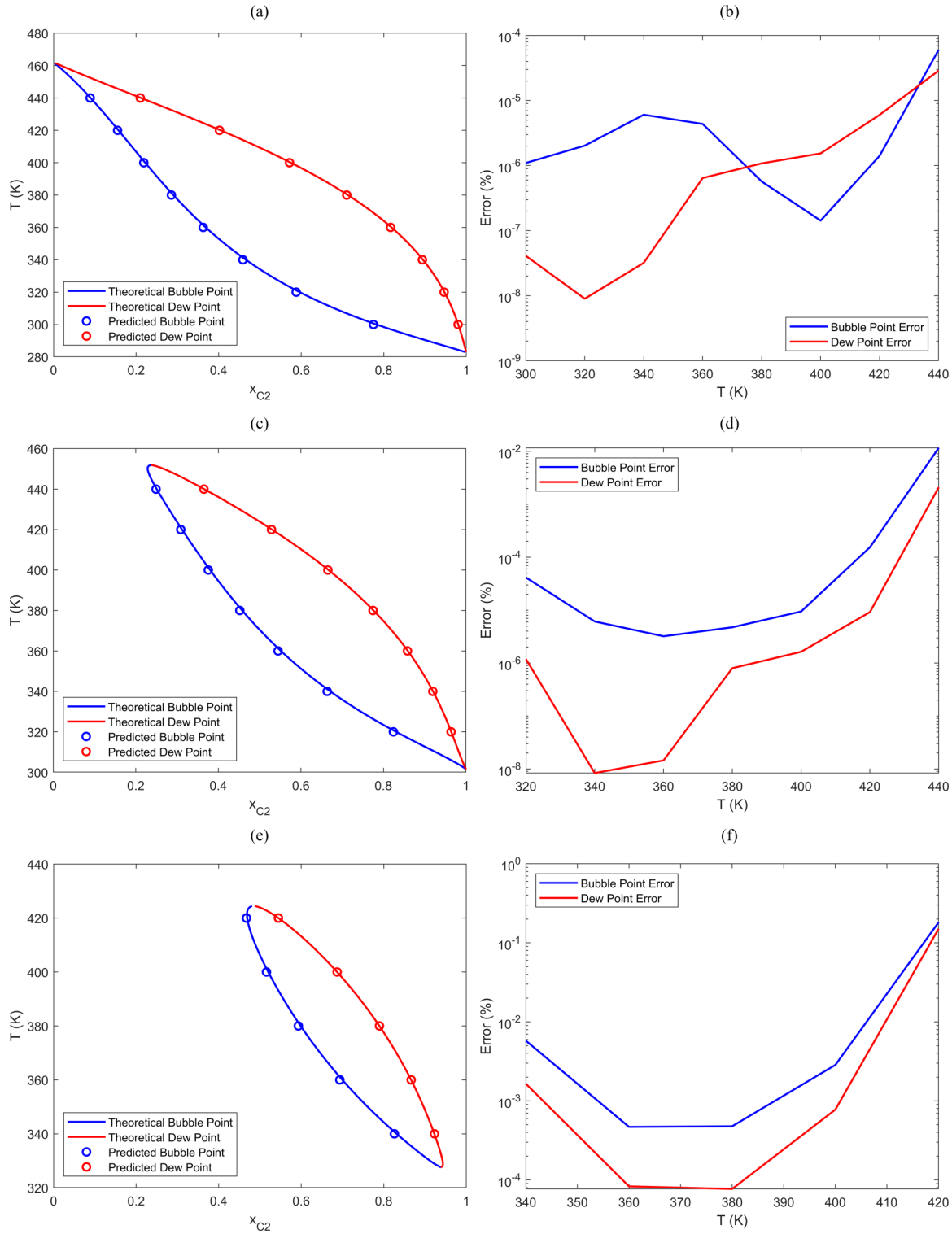

FIG. 6. Left: The T-x envelopes at (a) $p = 30$ bar, (c) $p = 45$ bar, and (e) $p = 58$ bar, where the solid lines represent the theoretical results and the dots represent the results predicted by LBM. Right: The relative error (%) in the predicted values at (b) $p = 30$ bar, (d) $p = 45$ bar, and (f) $p = 58$ bar.

20.684 bar. The density is initialized using Eq. (26), with $W = 4$ and $\rho_{i,V}$, $\rho_{i,L}$, and S_V calculated by performing a flash calculation using the PR EOS at 216.483 K and 20.684 bar. The simulation is run for 1 000 000 time steps until equilibrium is reached. The results of density and composition versus dimensionless length (x/n_x) are shown in Fig. 7. The results from a flash calculation at the temperature and updated pressure at the equilibrium state are also included in Fig. 7.

The deviation of the results of the fugacity-based LBM from the results of the flash calculation is quantified with a relative error [Eq. (27)] and tabulated in Table IV. The low

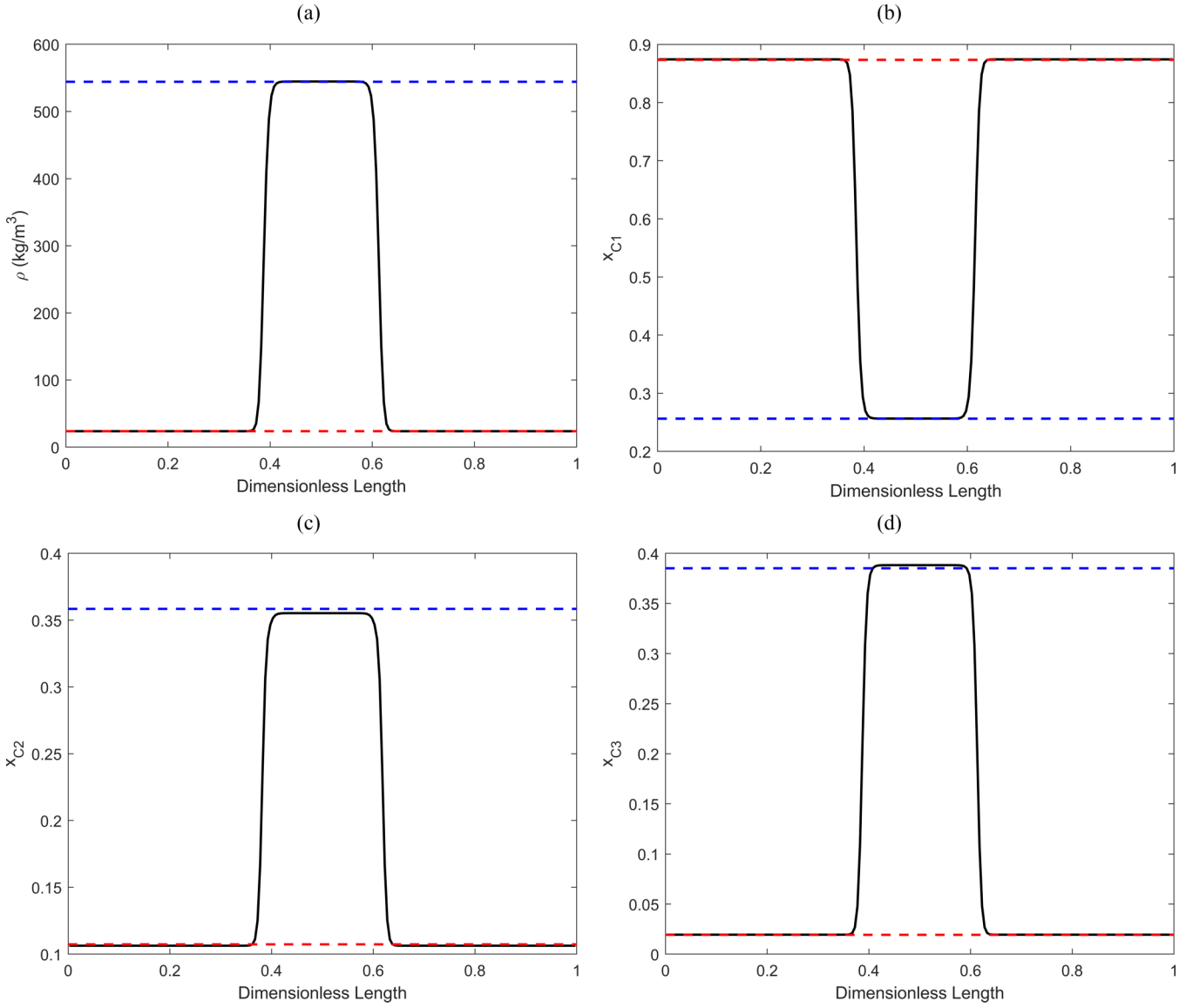

FIG. 7. The equilibrium profiles for the (a) density, (b) composition of C1, (c) composition of C2, and (d) composition of C3. The solid black line shows the results from LBM and the dashed blue and red lines show the theoretical values from a flash calculation for the liquid and vapor phase, respectively.

error values show that the fugacity-based LBM also predicts the correct values for multicomponent mixtures.

D. Spinodal decomposition

So far, we have shown results of our method initialized at equilibrium conditions, using Eq. (26). In this section, we show that our model allows for phase separation, in agreement with thermodynamics, when initialized far from equilibrium. To do this we simulate a case of spinodal decomposition of a system with ethane (C2) and *n*-pentane (C5), using the PR EOS. The size of the computational domain is 200×200 ($n_x \times n_y$), the relaxation time $\tau = 1.15$, and the values of interfacial tension strength are $\kappa_{C2} = 0.10$ and $\kappa_{C5} = 0.15$. The temperature in the domain is 387.70 K. The initial composition in the domain is kept uniform at $x_{C2} = 0.62$ and $x_{C5} = 0.38$ and the density is also kept uniform and such that the pressure in the domain is 50 bar. As can be seen in Fig. 5(c), at these conditions the domain should decompose into two separate phases. To trigger this decomposition, we introduce a random fluctuation in the total density of the system, and run the simulation for 500 000 time steps. The evolution of the total density with

TABLE IV. The relative error values in the density, C1 composition, C2 composition, and C3 composition in the different phases.

Property	Liquid region error (%)	Vapor region error (%)
Density	0.0705	0.0677
x_{C1}	0.0521	0.0970
x_{C2}	0.8962	0.9207
x_{C3}	0.7994	0.7320

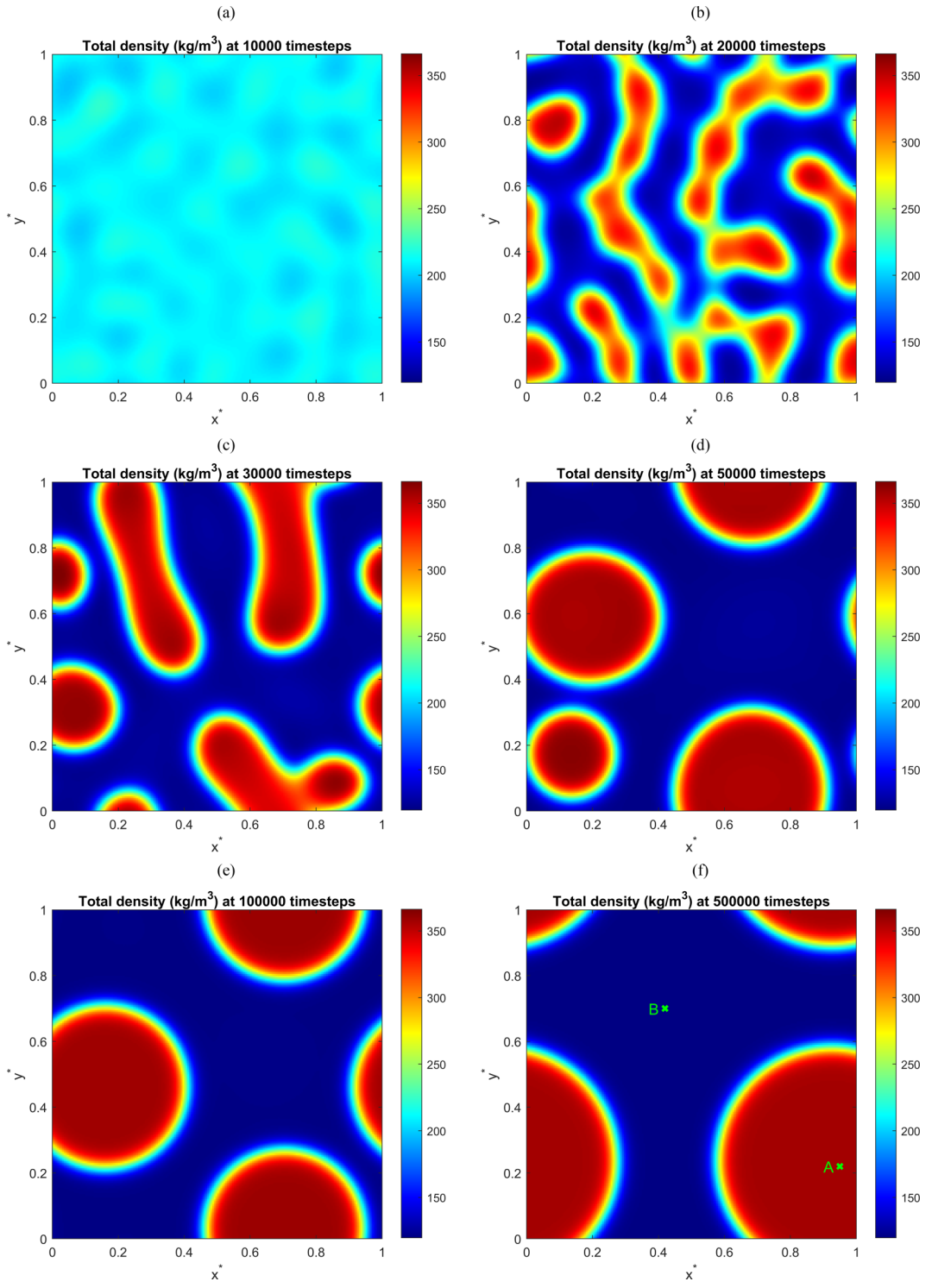

FIG. 8. A uniform system separating into different phases shown at time (in lattice units) (a) 10 000, (b) 20 000, (c) 30 000, (d) 50 000, (e) 100 000, and (f) 500 000. The points marked A and B, in (f), represent the points in the liquid and vapor region, respectively, where relevant properties are measured.

time is shown in Fig. 8. In these plots, the domain is characterized in terms of dimensionless lengths $x^* = x/n_x$ and $y^* = y/n_y$.

Figure 8 confirms that our model allows for phase separation of a domain initialized far from equilibrium. Now we test whether the results are consistent with thermodynamics. It should be noted that in Secs. IV A, IV B, and IV C, to test for consistency with thermodynamics, the results from LBM were compared with results from a flash calculation. However, a flash calculation assumes a flat interface, therefore, we cannot use the same approach to verify the results in this section. Instead, we verify our results by testing the isofugacity cri-

TABLE V. The fugacity of each component measured in each phase.

Component	Fugacity in liquid phase (bar)	Fugacity in vapor phase (bar)
C2	35.1276	35.1262
C5	4.4563	4.4567

terion, which applies to both flat and curved interfaces and is the kernel of the flash calculation. The fugacity of each component in the liquid phase [obtained at point A marked in Fig. 8(f)] and the vapor phase [obtained at point B marked in Fig. 8(f)] is measured and tabulated in Table V. It can be seen that the fugacity of each component is the same in the liquid and vapor phase, which confirms that the isofugacity criterion holds and that the phase separation predicted by the fugacity-based LBM is consistent with thermodynamics.

E. Oscillating droplet

For all the tests done so far, we have verified results under static conditions and in this section, we will test our model at dynamic conditions. We simulate the case of an elliptical droplet oscillating due to the effects of surface tension, which has been used to benchmark single-component [42] and multicomponent LBM models [12]. For this case propane (C3) and *n*-pentane (C5) are simulated using the PR EOS. The size of the computational domain is 200×200 ($n_x \times n_y$), the relaxation time $\tau = 0.85$, and the values of interfacial tension strength are $\kappa_{C3} = 0.05$ and $\kappa_{C5} = 0.10$. The temperature of the system is set to 340 K and the density is initialized using Eq. (28),

$$\rho_i(x, y, t = 0) = \frac{\rho_{i,L} + \rho_{i,V}}{2} - \frac{\rho_{i,L} - \rho_{i,V}}{2} \tanh\left\{\frac{2\left[\sqrt{(x - x_c)^2 + (y - y_c)^2/h^2} - R_0\right]}{W}\right\}. \tag{28}$$

Here x_c and y_c are the x and y coordinates of the center of the droplet set to be $x_c = n_x/2$ and $y_c = n_y/2$. The parameters controlling the shape of the elliptical droplet are set to be $R_0 = 30$, $h = 0.9$, and $W = 4$. Additionally, $\rho_{i,V}$ and $\rho_{i,L}$ are calculated by performing a flash calculation using the PR EOS at $T = 340$ K and $p = 5$ bar, which corresponds to a density ratio of 50.97. With this initialization, the elliptical droplet will oscillate, and the time period of this oscillation can be determined theoretically, as shown in Eq. (29) [43],

$$T_a = 2\pi\left[n(n^2 - 1)\frac{\sigma}{\rho_L R_e^3}\right]^{-1/2}. \tag{29}$$

Here T_a is the time period of the oscillations, n is the mode of oscillation ($n = 2$ for this case), σ is the interfacial tension and R_e is the equilibrium radius given by $R_e = \sqrt{R_{\max} R_{\min}}$, with $R_{\max} = R_0$ and $R_{\min} = R_0 h$. The simulation is run for 4000 time steps, and the ratio of the droplet radius to the equilibrium radius is plotted with time, along both the major and minor axis. It should be noted that the radius does not have a clear definition due to the presence of a diffuse interface and it is calculated by defining the boundary of the droplet to be the location where $\rho = (\rho_V + \rho_L)/2$. The location of this boundary is determined by linearly interpolation of the density distribution in space. This uncertainty in the radius introduces a scatter in the data extracted from the simulation, and the scatter is further amplified since we are capturing very small variations in the radius. Therefore, a smooth curve is fit to the data extracted from the simulation. The raw data and the smoothing curves are shown in Fig. 9. From Fig. 9, the period of the oscillations can be determined to be 1787.5 time steps (in lattice units), which agrees closely with the theoretical period of 1717.5 time steps, determined through Eq. (29),

V. DISCUSSION AND CONCLUSION

In this paper, we introduced a model for the free-energy LBM, which cannot only handle MCMP simulations of partially miscible fluids but is also able to incorporate any multicomponent EOS, without the need for any empirically determined tuning parameter to achieve full thermodynamic consistency. This model calculates the force required in the free-energy model for each component based on the fugacity of that component, a quantity readily available for any multicomponent EOS. Using this fugacity-based LBM model, we could show that accurate EOSs, like the PR and SRK equations, could easily be incorporated into LBM.

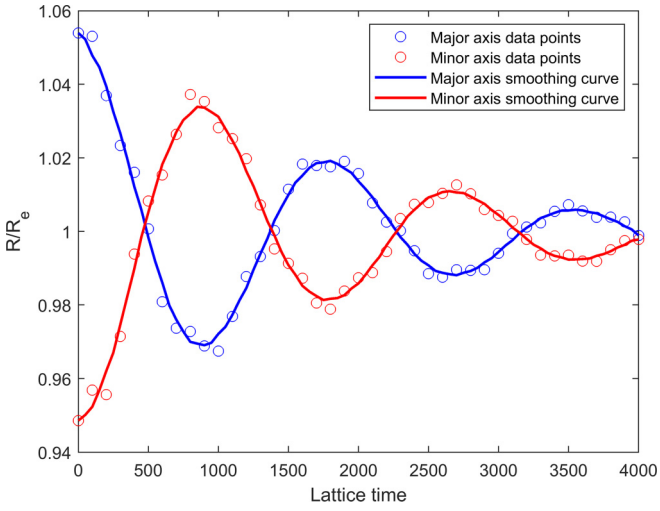

FIG. 9. The ratio of the droplet radius to the equilibrium radius versus time (in lattice units). The dots represent the raw data obtained from the simulation and the solid lines are the smooth curves fit to this data.

Additionally, we were able to use the fugacity-based LBM to extensively analyze a binary system's pressure, temperature, and composition behavior by replicating various characteristic pressure-composition and temperature-composition envelopes. We further showed that the fugacity-based LBM model could be applied to any number of components. All results from the fugacity-based LBM showed excellent agreement with the results predicted by multicomponent thermodynamics, with deviations well below 1%. We also tested the case of spinodal decomposition for a binary mixture and showed that a uniform system could decompose into two phases, in agreement with thermodynamics. Finally, we tested the model under dynamic conditions by simulating the case of an oscillating droplet and showing that the oscillation period obtained from the simulation agrees with the theoretical prediction.

A few things need to be stressed out about this procedure. First, our model is not restricted to the use of the well-balanced LBM formulation. It can apply to the standard LBM formulation, although there will be slight deviations from thermodynamic predictions. A general form of our proposed force for the standard multicomponent LBM would be given by Eq. (30),

$$\mathbf{F}_i = -\tilde{\rho}_i RT \nabla \ln f_i - \tilde{\rho}_i \nabla \mu_{I,i} + c_s^2 \nabla \rho_i. \tag{30}$$

Second, the well-balanced LBM is unstable at low relaxation time values and high density ratios. This problem can be addressed with a more stable version of the well-balanced LBM as shown in Ref. [22]. Third, the interfacial tension in our model is set indirectly, through the parameter κ_i. While the interfacial tension cannot be obtained beforehand, it can be calculated for a curved interface through the Young-Laplace test or for a flat interface by integrating the difference between the normal and transversal components of the pressure tensor across the interface, resulting in Eq. (31) [44]. Both of these approaches would require knowing simulation results,

$$\sigma = \int_{-\infty}^{+\infty} \left[\sum_{i=1}^{N_c} \sum_{j=1}^{N_c} \kappa_{ij} \frac{d\tilde{\rho}_i}{dx} \frac{d\tilde{\rho}_j}{dx} \right] dx. \tag{31}$$

Last, the expression for fugacity is generally written with dimensionless groups inside the natural logs as shown in Eqs (C15), (C16), and (C17) in Appendix C. This way of calculating fugacity could potentially lead to instabilities as the pressure can take on a negative value in the interface region which can cause the term $\ln[(\tilde{v} - b_m)p/(RT)]$ to turn into a log of a negative number. This term will appear in the fugacity expression for any EOS. To avoid this, we recommend calculating the natural log of the fugacity at each node as shown in Eq. (32) for the vdW EOS, Eq. (33) for the SRK EOS, or Eq. (34) for the PR EOS. Then Eq. (23) can be used with the natural log of the fugacity to calculate the component force,

$$\ln f_i = \ln x_i + \frac{b_i}{\tilde{v} - b_m} - \ln\left[\frac{(\tilde{v} - b_m)}{RT}\right] - \frac{2}{RT\tilde{v}} \sum_{j=1}^{N_c} x_j a_{ij}, \tag{32}$$

$$\ln f_i = \ln x_i + \frac{b_i}{b_m}\left[\frac{p\tilde{v}}{RT} - 1\right] - \ln\left[\frac{(\tilde{v} - b_m)}{RT}\right] + \frac{(a\alpha)_m}{b_m RT}\left[\frac{b_i}{b_m} - \frac{2}{(a\alpha)_m} \sum_{j=1}^{N_c} x_j (a\alpha)_{ij}\right] \ln\left[1 + \frac{b_m}{\tilde{v}}\right], \tag{33}$$

$$\ln f_i = \ln x_i + \frac{b_i}{b_m}\left[\frac{p\tilde{v}}{RT} - 1\right] - \ln\left[\frac{(\tilde{v} - b_m)}{RT}\right] + \frac{(a\alpha)_m}{2\sqrt{2}b_m RT}\left[\frac{b_i}{b_m} - \frac{2}{(a\alpha)_m} \sum_{j=1}^{N_c} x_j (a\alpha)_{ij}\right] \ln\left[\frac{\tilde{v} + (1+\sqrt{2})b_m}{\tilde{v} + (1-\sqrt{2})b_m}\right]. \tag{34}$$

ACKNOWLEDGMENTS

Funding support from the William A. Fustos Family Professorship in Energy and Mineral Engineering at the Pennsylvania State University is gratefully acknowledged.

APPENDIX A: PITFALLS OF DERIVING FREE ENERGY FROM AN EQUATION OF STATE

In this study, we propose to create a multicomponent LBM model that does not rely on deriving the free-energy functional from an EOS, as is done for single-component models. To see why deriving the free-energy functional from an EOS would not work in a multicomponent case, we start by writing the total differential of the Helmholtz free energy given by Eq. (A1),

$$d\Psi = -SdT - pdV + \sum_{i=1}^{N_c} \mu_i dn_i. \tag{A1}$$

Here S is the entropy. We can identify that the pressure is the negative partial derivative of the free energy with respect to volume as shown in Eq. (A2),

$$p = -\left(\frac{\partial \Psi}{\partial V}\right)_{T,n_i}. \tag{A2}$$

Since the free energy is mathematically homogeneous, we can derive an intensive free energy per unit mole, $\tilde{\psi}$, through Eq. (A3). In the literature, the intensive free energy is usually defined per unit volume; however, it carries the same information as if were defined per unit mole and in this case, it would simplify the calculations,

$$\tilde{\psi}\left(T, \frac{V}{n}, \frac{n_i}{n}\right) = \tilde{\psi}(T, \tilde{v}, x_i) = \frac{\Psi(T, V, n_i)}{n}. \tag{A3}$$

Here $\tilde{v}$ is the volume per unit mole (molar volume). The pressure can then be written as shown in Eq. (A4),

$$p = -\left(\frac{\partial \tilde{\psi}}{\partial \tilde{v}}\right)_{T,x_i}. \tag{A4}$$

Integrating Eq. (A4) at constant temperature and composition the molar free energy will be given by Eq. (A5a) and the extensive free energy will be given by Eq. (A5b),

$$\tilde{\psi} = -\int p d\tilde{v} + C(T, x_i), \tag{A5a}$$

$$\Psi = -n\int p d\tilde{v} + nC(T, x_i). \tag{A5b}$$

Here C is a constant of integration which is a function of temperature and composition. The chemical potential of component i is the partial derivative of the free energy with respect to the moles of component i; therefore, it will be given by Eq. (A6),

$$\mu_i = \frac{\partial}{\partial n_i}\left[-n\int p d\tilde{v}\right]_{T,V,n_{j\neq i}} + \frac{\partial}{\partial n_i}[nC(T, x_i)]_{T,V,n_{j\neq i}}. \tag{A6}$$

The first term on the left-hand side of Eq. (A6) can be evaluated with an EOS, whereas the second term is unknown. For a single-component, isothermal simulation, this constant of integration can be ignored as we are interested in the gradient of chemical potential, which will be calculated as follows:

$$\mu = \frac{\partial}{\partial n}\left[-n\int p d\tilde{v}\right]_{T,V} + \frac{\partial}{\partial n}[nC(T)]_{T,V}$$

$$\mu = \frac{\partial}{\partial n}\left[-n\int p d\tilde{v}\right]_{T,V} + C(T)$$

$$\nabla\mu = \nabla\left[\frac{\partial}{\partial n}\left(-n\int p d\tilde{v}\right)_{T,V}\right].$$

However, this cannot be done for a multicomponent case since the constant of integration is a function of temperature and composition, and therefore it cannot be ignored.

APPENDIX B: PITFALLS OF DERIVING FREE ENERGY FROM THE CANONICAL PARTITION FUNCTION

The van der Waals EOS has a firm footing in statistical mechanics. In this Appendix, we will show how a free-energy functional can be derived for a van der Waals fluid from the canonical partition function. We will also show how this cannot be extended to other EOSs, and hence the need for our proposed model. The canonical partition function, Q, for a system is given by Eq. (B1) [38],

$$Q = \frac{Q_{\text{int}}^N}{N!\Lambda^{3N}}\int_{\mathbf{r}^N}\exp\left(-\frac{U}{k_BT}\right)d\mathbf{r}^N. \tag{B1}$$

Here N is the number of molecules in the system, k_B is the Boltzmann constant, Q_{int} is the contribution of the partition function due to the internal structure of the molecules, U is the total potential energy of the system, and $\Lambda = \sqrt{h^2/(2\pi m k_B T)}$ is the thermal de Broglie wavelength, with h being the Planck's constant and m being the mass of a molecule. $\mathbf{r}^N$ is the collection of the position vector of each molecule, $\mathbf{r}_i$, in the system such that:

$$d\mathbf{r}^N = d\mathbf{r}_1 d\mathbf{r}_2, \ldots, d\mathbf{r}_N.$$

The potential energy of the system is dependent of the position of every single molecule in the system; however, it can be approximated as a position-independent mean potential energy, $\bar{U}$. The canonical partition function can then be written as shown in Eq. (B2),

$$Q = \frac{Q_{\text{int}}^N}{N!\Lambda^{3N}}\exp\left(-\frac{\bar{U}}{k_BT}\right)\int_{\mathbf{r}^N} d\mathbf{r}^N. \tag{B2}$$

The integral in Eq. (B2) is simply a volume integral evaluated N times. If the molecules are assumed as hard spheres, then the volume available for the molecules to move will have to account for the excluded volume due to the volume of the molecules. The available volume is $(V - N\bar{b})$, where $\bar{b}$ is the excluded volume per molecule and therefore, Eq. (B2) becomes Eq. (B3),

$$Q = \frac{Q_{\text{int}}^N}{N!\Lambda^{3N}}(V - N\bar{b})^N\exp\left(-\frac{\bar{U}}{k_BT}\right). \tag{B3}$$

The free energy is given by $\Psi = -k_BT\ln Q$. Therefore, the free-energy functional can be written as shown in Eq. (B4),

$$\Psi = -Nk_BT\ln(V - N\bar{b}) + \bar{U} + Nk_BT(\ln N - 1) + 3Nk_BT\ln\Lambda - Nk_BT\ln Q_{\text{int}}. \tag{B4}$$

Using an intermolecular pair potential based on hard sphere repulsion and Lennard-Jones type attraction, the mean potential energy can be approximated as shown in Eq. (B5) [38],

$$\bar{U} = -\bar{a}\frac{N^2}{V}. \tag{B5}$$

Here $\bar{a}$ is the attraction term in an EOS when written for the number of molecules and not the number of moles. The free-energy functional will then be given by Eq. (B6),

$$\Psi = -Nk_BT\ln(V - N\bar{b}) - \bar{a}\frac{N^2}{V} + Nk_BT(\ln N - 1) + 3Nk_BT\ln\Lambda - Nk_BT\ln Q_{\text{int}}. \tag{B6}$$

The pressure can be computed from the partial derivative of the free energy as follows:

$$p = -\left(\frac{\partial\Psi}{\partial V}\right)_{T,N}.$$

Keeping in mind that Q_{int} and Λ are not functions of volume, the pressure is given by Eq. (B7),

$$p = \frac{Nk_BT}{V - N\bar{b}} - \bar{a}\frac{N^2}{V^2}. \tag{B7}$$

When written in terms of moles, using the a and b for the attraction parameter and covolume respectively ($a = \bar{a}N_A^2$ and $b = \bar{b}N_A$, where N_A is the Avogadro constant), Eq. (B7) is the van der Waals EOS [Eq. (B8)],

$$p = \frac{RT}{\tilde{v} - b} - \frac{a}{\tilde{v}^2}, \tag{B8}$$

The free energy given by Eq. (B6) is the free energy of a van der Waals fluid. More recent cubic EOSs are empirical modifications to the van der Waals EOS and have the same

form. They can be generalized as shown in Eq. (B9),

$$p = \frac{RT}{\tilde{v} - b} + p_{\text{att}}. \tag{B9}$$

Here p_{att} is the contribution of the attractive interactions between molecules to the pressure. For the van der Waals EOS $p_{\text{att}} = -a/\tilde{v}^2$, for the PR EOS $p_{\text{att}} = -a\alpha/(\tilde{v}^2 + 2b\tilde{v} - b^2)$ and for the SRK EOS $p_{\text{att}} = -a\alpha/(\tilde{v}^2 + b\tilde{v})$. These EOSs will be discussed in detail in Appendix C. It can be seen that p_{att} emerges from the mean potential energy of the system [Eq. (B5)]. The relationship between p_{att} and $\bar{U}$ is given by Eq. (B10),

$$p_{\text{att}} = -\left(\frac{\partial \bar{U}}{\partial V}\right)_{T,n}. \tag{B10}$$

The free-energy functional can be written for any EOS by integrating Eq. (B10) and substituting into Eq. (B4). However, integrating Eq. (B10) would introduce a constant of integration which is a function of the temperature and moles, $C(T, n)$, as shown in Eq. (B11),

$$\begin{aligned}\Psi \quad &= -Nk_BT \ln(V - N\bar{b}) - \int p_{\text{att}} dV + C(T, n) \\ &+ Nk_BT(\ln N - 1) + 3Nk_BT \ln \Lambda - Nk_BT \ln Q_{\text{int}}.\end{aligned} \tag{B11}$$

For the free-energy LBM, we require an expression for the chemical potential for which we need to take the partial derivative of the free-energy functional with respect to the moles. The constant of integration would affect the results when taking this partial derivative and hence a unique chemical potential cannot be obtained. This constant of integration cannot be designed for a particular EOS as any choice of $C(T, n)$ will retrieve that EOS (the EOS is retrieved by taking a partial derivative of the free-energy functional with respect to volume and the constant of integration is not a function of volume). However, there is no way of gauging the effect of the designed $C(T, n)$ on the chemical potential. Therefore, EOSs like the PR and SRK cannot be incorporated into our model the same way as the van der Waals EOS.

APPENDIX C: COMMON EQUATIONS OF STATE AND THEIR RESPECTIVE FUGACITY EXPRESSIONS

1. Equations of state

A popular class of EOSs is cubic EOSs. In this Appendix, we will go through some important cubic EOSs and their extensions to multicomponent mixtures. For a pure component i, a cubic EOS has a parameter accounting for molecular attraction, a_i or $(a\alpha)_i$, and a parameter accounting for the volume occupied by the molecules, b_i (also known as the covolume). For the case of a multicomponent mixture, these pure component parameters are replaced with mixture parameters: a_m or $(a\alpha)_m$ and b_m. The mixture parameters are calculated using van der Waals mixing rules by considering attractions between like and unlike component pairs and an average molecular volume [3]. The first cubic EOS was the vdW EOS [45]. Two extensions of the vdW EOS known for their accuracy are the SRK [2] and PR [1] EOS. The multicomponent vdW, SRK, and PR EOS are summarized in the following sections.

a. vdW equation of state

The vdW EOS is given by Eq. (C1),

$$p = \frac{RT}{\tilde{v} - b_m} - \frac{a_m}{\tilde{v}^2}. \tag{C1}$$

Here p is the pressure, R is the universal gas constant, T is the temperature, and $\tilde{v}$ is the molar volume. For a mixture with N_c components, the mixing rules for the attraction term and covolume term are given by Eq. (C2) and Eq. (C3), respectively,

$$a_m = \sum_{i=1}^{N_c}\sum_{j=1}^{N_c} x_i x_j a_{ij}, \tag{C2a}$$

$$a_{ij} = \sqrt{a_i a_j}(1 - \delta_{ij}), \tag{C2b}$$

$$b_m = \sum_{i=1}^{N_c} x_i b_i. \tag{C3}$$

Here x_i is the mole fraction of component i and δ_{ij} is the binary interaction parameter between component i and component j. The attraction and covolume terms for component i are given by $a_i = \frac{27}{64}\frac{R^2T_{c,i}^2}{P_{c,i}}$ and $b_i = \frac{1}{8}\frac{RT_{c,i}}{P_{c,i}}$ and $T_{c,i}$ and $P_{c,i}$ are the critical temperature and critical pressure of component i respectively.

b. SRK equation of state

The SRK EOS is given by Eq. (C4),

$$p = \frac{RT}{\tilde{v} - b_m} - \frac{(a\alpha)_m}{\tilde{v}(\tilde{v} + b_m)}. \tag{C4}$$

For a mixture with N_c components, the mixing rules for the attraction term and covolume term are given by Eq. (C5) and Eq. (C3), respectively,

$$(a\alpha)_m = \sum_{i=1}^{N_c}\sum_{j=1}^{N_c} x_i x_j (a\alpha)_{ij}, \tag{C5a}$$

$$(a\alpha)_{ij} = \sqrt{(a\alpha)_i (a\alpha)_j}(1 - \delta_{ij}). \tag{C5b}$$

Here $a_i = 0.4274802\frac{R^2T_{c,i}^2}{P_{c,i}}$, $b_i = 0.08664035\frac{RT_{c,i}}{P_{c,i}}$, and

$$\alpha_i = \left[1 + \left(0.48 + 1.574\omega_i - 0.176\omega_i^2\right)\left(1 - T_{r,i}^{0.5}\right)\right]^2,$$

where ω_i is the accentric factor of component i and $T_{r,i} = \frac{T}{T_{c,i}}$.

c. PR equation of state

The PR EOS is given by Eq. (C6),

$$p = \frac{RT}{\tilde{v} - b_m} - \frac{(a\alpha)_m}{\tilde{v}^2 + 2b_m\tilde{v} - b_m^2}. \tag{C6}$$

For a mixture with N_c components, the mixing rules for the attraction term and covolume term are given by Eq. (C5)

and Eq. (C3), respectively, with $a_i = 0.457235529\frac{R^2T_{c,i}^2}{P_{c,i}}$, $b_i = 0.077796074\frac{RT_{c,i}}{P_{c,i}}$, and

$$\alpha_i = \begin{cases} \left[1 + \left(0.374640 + 1.54226\omega_i - 0.26992\omega_i^2\right)\left(1 - T_{r,i}^{0.5}\right)\right]^2 & \text{if } \omega_i \leqslant 0.49 \\ \left[1 + \left(0.379642 + 1.48503\omega_i - 0.164423\omega_i^2 + 0.016666\omega_i^3\right)\left(1 - T_{r,i}^{0.5}\right)\right]^2 & \text{if } \omega_i > 0.49 \end{cases}.$$

2. Fugacity expressions from relevant equations of state

In this Appendix, we will show how to derive an expression for the fugacity using its definition given by Eq. (19). Then we will show how this expression can be evaluated using the vdW, SRK, and PR EOS. To obtain an expression for the fugacity of component i we start by integrating Eq. (19a) by varying the pressure while keeping temperature and composition constant to obtain Eq. (C7),

$$\ln\left[f_i(T, p, x_i)\right] - \ln\left[f_i(T, p^{\text{ref}}, x_i)\right] = \frac{\mu_{B,i}(T, p, x_i) - \mu_{B,i}(T, p^{\text{ref}}, x_i)}{RT}. \tag{C7}$$

Here x_i is the mole fraction for component i and p^{ref} is the reference pressure for integration. Taking the reference pressure to be approaching 0, $p^{\text{ref}} = p_0$, we can use the reference state given by Eq. (19b) [$f_i(T, p_0, x_i) = x_i p_0$]. Additionally, at low pressure, the mixture behaves like an ideal gas mixture (denoted by superscript IGM). Therefore, we get Eq. (C8),

$$\ln\left[f_i(T, p, x_i)\right] - \ln\left[x_i p_0\right] = \frac{\mu_{B,i}(T, p, x_i) - \mu_{B,i}^{\text{IGM}}(T, p_0, x_i)}{RT}. \tag{C8}$$

For an ideal gas mixture, Eq. (C9) holds [46],

$$\mu_{B,i}^{\text{IGM}}(T, p, x_i) - \mu_{B,i}^{\text{IGM}}(T, p_0, x_i) = RT\ln\frac{p}{p_0}. \tag{C9}$$

Combining Eqs. (C8) and (C9) we get:

$$\ln\left[\frac{f_i(T, p, x_i)}{x_i p}\right] = \mu_{B,i}(T, p, x_i) - \mu_{B,i}^{\text{IGM}}(T, p, x_i). \tag{C10}$$

The right-hand side of Eq. (C10) is the residual chemical potential which can be evaluated to give Eq. (C11) [46],

$$\ln\left[\frac{f_i(T, p, x_i)}{x_i p}\right] = \frac{1}{RT}\int_0^p \left[\left(\frac{\partial V}{\partial n_i}\right)_{T,p,n_{j\neq i}} - \frac{RT}{p}\right] dp. \tag{C11}$$

Here n_i is the moles of component i and V is the volume. Applying the cyclic rule for the properties p, V, and n_i holding T and $n_{j\neq i}$ constant, we get:

$$\left(\frac{\partial V}{\partial n_i}\right)_{T,p,n_{j\neq i}}\left(\frac{\partial p}{\partial V}\right)_{T,n_i}\left(\frac{\partial n_i}{\partial p}\right)_{T,V,n_{j\neq i}} = -1. \tag{C12}$$

The integral in Eq. (C11) is at constant temperature and composition, and therefore the term $(\frac{\partial p}{\partial V})_{T,n_i}$ in Eq. (C12) will turn into a total derivative giving Eq. (C13) [47],

$$\left(\frac{\partial V}{\partial n_i}\right)_{T,p,n_{j\neq i}} dp = -\left(\frac{\partial p}{\partial n_i}\right)_{T,V,n_{j\neq i}} dV. \tag{C13}$$

Substituting into Eq. (C11):

$$\ln\left[\frac{f_i(T, p, x_i)}{x_i p}\right] = -\frac{1}{RT}\int_\infty^V \left[\left(\frac{\partial p}{\partial n_i}\right)_{T,V,n_{j\neq i}}\right] dV - \frac{1}{RT}\int_0^p \left[\frac{RT}{p}\right] dp. \tag{C14}$$

The partial derivative $(\frac{\partial p}{\partial n_i})_{T,V,n_{j\neq i}}$ can be evaluated using a pressure explicit EOS, like Eqs. (C1), (C4), or (C6). While evaluating this derivative, the composition in the EOS needs to be expressed as $x_i = \frac{n_i}{\sum_i n_i}$ and molar volume needs to be expressed as $\tilde{v} = \frac{V}{\sum_i n_i}$. Then Eq. (C14) can be solved to find the fugacity of component i. The fugacity expression for the vdW, SRK and PR EOS are given by Eqs. (C15), (C16), and (C17), respectively [47,48],

$$\ln\left[\frac{f_i}{x_i p}\right] = \frac{b_i}{\tilde{v} - b_m} - \ln\left[\frac{(\tilde{v} - b_m)p}{RT}\right] - \frac{2}{RT\tilde{v}}\sum_{j=1}^{N_c} x_j a_{ij}, \tag{C15}$$

$$\ln\left[\frac{f_i}{x_i p}\right] = \frac{b_i}{b_m}\left[\frac{p\tilde{v}}{RT} - 1\right] - \ln\left[\frac{(\tilde{v} - b_m)p}{RT}\right] + \frac{(a\alpha)_m}{b_m RT}\left[\frac{b_i}{b_m} - \frac{2}{(a\alpha)_m}\sum_{j=1}^{N_c} x_j(a\alpha)_{ij}\right]\ln\left[1 + \frac{b_m}{\tilde{v}}\right], \tag{C16}$$

$$\ln\left[\frac{f_i}{x_i p}\right] = \frac{b_i}{b_m}\left[\frac{p\tilde{v}}{RT} - 1\right] - \ln\left[\frac{(\tilde{v} - b_m)p}{RT}\right] + \frac{(a\alpha)_m}{2\sqrt{2}b_m RT}\left[\frac{b_i}{b_m} - \frac{2}{(a\alpha)_m}\sum_{j=1}^{N_c} x_j(a\alpha)_{ij}\right]\ln\left[\frac{\tilde{v} + (1 + \sqrt{2})b_m}{\tilde{v} + (1 - \sqrt{2})b_m}\right]. \tag{C17}$$

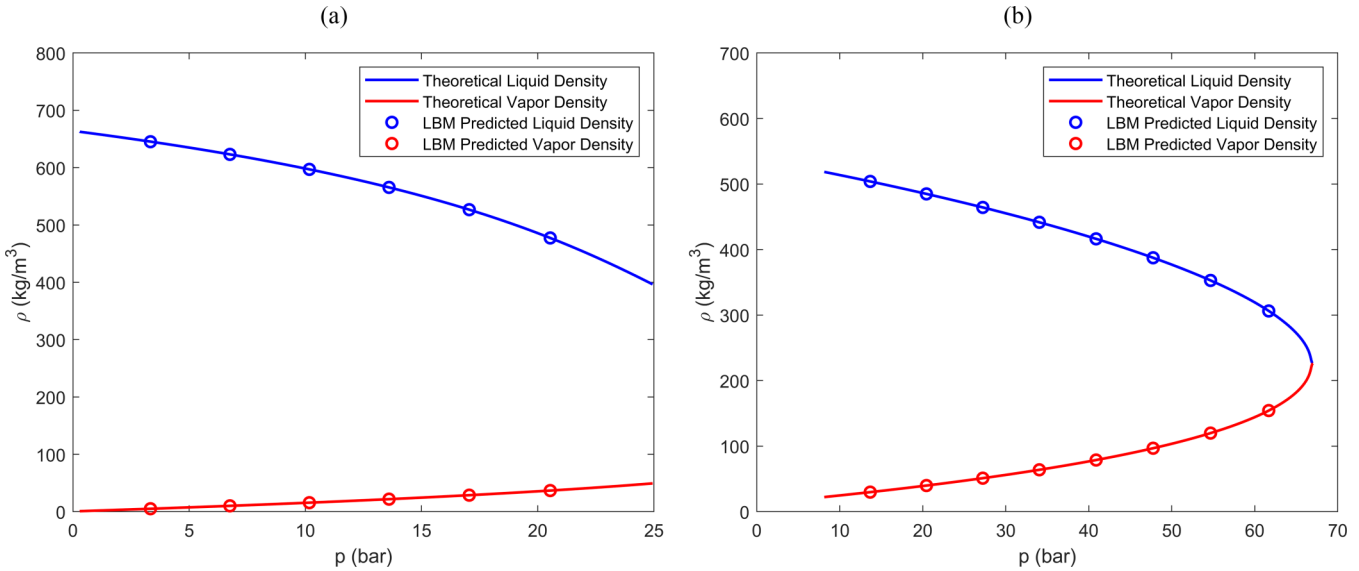

FIG. 10. The liquid density vs pressure (blue) and vapor density vs pressure (red) at (a) $T = 274.96$ K and (b) $T = 387.70$ K. The solid lines represent the theoretical results, whereas the dots represent the results predicted by LBM.

APPENDIX D: DENSITY VERSUS PRESSURE AND DENSITY VS TEMPERATURE PLOTS FROM SECTION IV B

Several vapor-liquid equilibrium cases were simulated in Sec. IV B to obtain the p-x and T-x envelopes. The density of the vapor phase and the density of the liquid phase at each of the pressures the simulations were run at to generate the p-x envelope are plotted in Fig. 10. The theoretical vapor and liquid phase densities predicted by a flash calculation are also shown.

The density of the vapor phase and the density of the liquid phase at each of the temperatures the simulations were run at to generate the T-x envelope are plotted in Fig. 11. The theoretical vapor and liquid phase densities predicted by a flash calculation are also shown. In this figure, we see a greater deviation of the LBM results from the theoretical results and this is because the theoretical results are generated at a constant pressure where as the equilibrium pressure in LBM slightly varies, as discussed in Sec. IV B in reference to the T-x envelopes from Fig. 6.

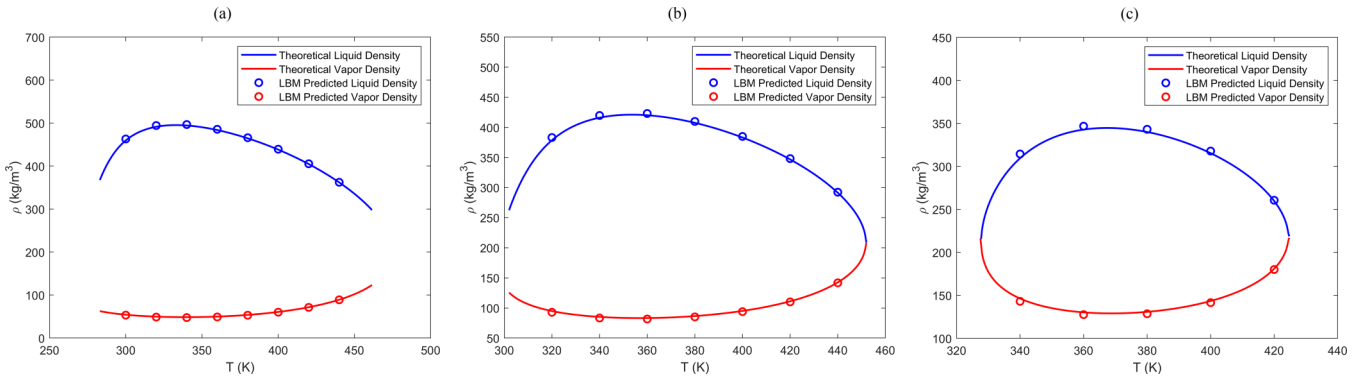

FIG. 11. The liquid density vs temperature (blue) and vapor density vs temperature (red) at (a) $p = 30$ bar, (b) $p = 45$ bar, and (c) $p = 58$ bar. The solid lines represent the theoretical results whereas the dots represent the results predicted by LBM.

[1] D.-Y. Peng and D. B. Robinson, Ind. Eng. Chem. Fund. **15**, 59 (1976).
[2] G. Soave, Chem. Eng. Sci. **27**, 1197 (1972).
[3] T. Kwak and G. Mansoori, Chem. Eng. Sci. **41**, 1303 (1986).
[4] G. N. Lewis, Proc. Am. Acad. Arts Sci. **37**, 49 (1901).
[5] D. H. Rothman and J. M. Keller, J. Stat. Phys. **52**, 1119 (1988).
[6] X. Shan and H. Chen, Phys. Rev. E **47**, 1815 (1993).
[7] M. R. Swift, W. R. Osborn, and J. M. Yeomans, Phys. Rev. Lett. **75**, 830 (1995).
[8] P. Yuan and L. Schaefer, Phys. Fluids **18**, 042101 (2006).
[9] N. S. Martys and H. Chen, Phys. Rev. E **53**, 743 (1996).
[10] J. Bao and L. Schaefer, Appl. Math. Model. **37**, 1860 (2013).
[11] X. He and G. D. Doolen, J. Stat. Phys. **107**, 309 (2002).
[12] C. Peng, L. F. Ayala, and O. M. Ayala, J. Comput. Phys. **429**, 110018 (2021).
[13] C. Peng, L. F. Ayala, Z. Wang, and O. M. Ayala, Phys. Rev. E **101**, 063309 (2020).
[14] L. E. Czelusniak, V. P. Mapelli, A. J. Wagner, and L. Cabezas-Gómez, Phys. Rev. E **105**, 015303 (2022).
[15] L.-S. Luo, Phys. Rev. Lett. **81**, 1618 (1998).
[16] Z. Guo, C. Zheng, and B. Shi, Phys. Rev. E **83**, 036707 (2011).
[17] Z. Guo, Phys. Fluids **33**, 031709 (2021).
[18] A. Mazloomi M, S. S. Chikatamarla, and I. V. Karlin, Phys. Rev. Lett. **114**, 174502 (2015).
[19] A. Mazloomi M., S. S. Chikatamarla, and I. V. Karlin, Phys. Rev. E **92**, 023308 (2015).
[20] D. N. Siebert, P. C. Philippi, and K. K. Mattila, Phys. Rev. E **90**, 053310 (2014).
[21] B. Wen, L. Zhao, W. Qiu, Y. Ye, and X. Shan, Phys. Rev. E **102**, 013303 (2020).
[22] C. Zhang, Z. Guo, and L.-P. Wang, Phys. Fluids **34**, 012110 (2022).
[23] Z. Qiao, X. Yang, and Y. Zhang, Int. J. Heat Mass Transf. **141**, 1216 (2019).
[24] H. Liu, Q. Kang, C. R. Leonardi, S. Schmieschek, A. Narváez, B. D. Jones, J. R. Williams, A. J. Valocchi, and J. Harting, Comput. Geosci. **20**, 777 (2016).
[25] L. Scarbolo, D. Molin, P. Perlekar, M. Sbragaglia, A. Soldati, and F. Toschi, J. Comput. Phys. **234**, 263 (2013).
[26] H. Liang, B. C. Shi, and Z. H. Chai, Phys. Rev. E **93**, 013308 (2016).
[27] A. Lamura, G. Gonnella, and J. M. Yeomans, Europhys. Lett. **45**, 314 (1999).
[28] X. Yuan, B. Shi, C. Zhan, and Z. Chai, Phys. Fluids **34**, 023311 (2022).
[29] L. Zheng, S. Zheng, and Q. Zhai, Phys. Rev. E **101**, 043302 (2020).
[30] C. Semprebon, T. Krüger, and H. Kusumaatmaja, Phys. Rev. E **93**, 033305 (2016).
[31] X. He and L.-S. Luo, Phys. Rev. E **56**, 6811 (1997).
[32] Z. Guo, C. Zheng, and B. Shi, Phys. Rev. E **65**, 046308 (2002).
[33] T. Krüger, H. Kusumaatmaja, A. Kuzmin, O. Shardt, G. Silva, and E. M. Viggen, *The Lattice Boltzmann Method: Principles and Practice* (Springer International Publishing, Cham, 2017), pp. 343–352.
[34] J. W. Cahn and J. E. Hilliard, J. Chem. Phys. **28**, 258 (1958).
[35] X. Fu, L. Cueto-Felgueroso, and R. Juanes, Phys. Rev. E **94**, 033111 (2016).
[36] X. Fu, L. Cueto-Felgueroso, and R. Juanes, Phys. Rev. Fluids **2**, 104001 (2017).
[37] K. S. Ridl and A. J. Wagner, Phys. Rev. E **98**, 043305 (2018).
[38] T. Hill, *An Introduction to Statistical Thermodynamics*, Dover Books on Physics (Dover, Mineola, NY, 2012), pp. 286–288.
[39] M. Wöhrwag, C. Semprebon, A. Mazloomi Moqaddam, I. Karlin, and H. Kusumaatmaja, Phys. Rev. Lett. **120**, 234501 (2018).
[40] J. Zhang and D. Y. Kwok, Eur. Phys. J.: Spec. Top. **171**, 45 (2009).
[41] J. Kim, Comput. Methods Appl. Mech. Eng. **196**, 4779 (2007).
[42] Q. Li, K. H. Luo, and X. J. Li, Phys. Rev. E **87**, 053301 (2013).
[43] H. Lamb, *Hydrodynamics* (Dover, Mineola, NY, 1932).
[44] B. S. Carey, L. E. Scriven, and H. T. Davis, AIChE J. **26**, 705 (1980).
[45] J. D. van der Waals, On the continuity of the gaseous and liquid states, Ph.D. thesis, Universiteit Leiden, 1873.
[46] S. Sandler, *Chemical, Biochemical, and Engineering Thermodynamics*, 4th ed. (John Wiley & Sons, New York, 2006), pp. 404–405.
[47] M. D. Koretsky, *Engineering and Chemical Thermodynamics* (John Wiley & Sons, New York, 2013), pp. 405–408.
[48] I. Tosun, *The Thermodynamics of Phase and Reaction Equilibria* (Elsevier, Amsterdam, 2013), pp. 239–243.